

**TICRA**  
**engineering consultants**  
communications systems and antennas

Planck Telescope  
RF Performance  
Independent Verification  
Phase 1

RF performance from measured mirrors

February, 2005

S-1287-07

Author: Per Heighwood Nielsen

## TABLE OF CONTENTS

1. INTRODUCTION	1
2. NOMINAL RF PERFORMANCE	2
3. MEASURED PRIMARY MIRROR	4
3.1 Measured surface	4
3.2 RF performance	8
4. MEASURED SECONDARY MIRROR	20
4.1 Measured surface	20
4.2 RF performance	24
5. COMBINED RF PERFORMANCE	36
REFERENCES	41

## 1. INTRODUCTION

The present study is prepared for ESTEC under contract no. 18395/04/NL/NB.

The title of the work is

Planck Telescope RF Performance Independent Verification

This Report presents the analysis of the manufactured Planck telescope mirrors and the corresponding RF degradation at 100 GHz. The RF performance of the nominal mirror system is presented for comparison in Chapter 2.

The Qualification model, QM, mirrors for the PLANCK telescope have now been manufactured and the surface accuracies have been measured. The measurement has been carried out by EADS-ASTRIUM after mechanical tests using an ordinary 3D measuring machine at room temperature and the results show that the accuracies are within the required tolerances. The measurements for the primary and the secondary mirror are dated 23.09.2004 and 15.09.2004, respectively

The separate analyses of the measured primary and the secondary mirror is performed in Chapter 3 and Chapter 4, respectively. The RF performance with both measured mirrors is given in Chapter 5.

## 2. NOMINAL RF PERFORMANCE

The patterns are presented in a  $\phi$ - $\theta$  grid around the main beam peak. The  $\phi, \theta$  direction angles are defined in an output coordinate system with its z-axis in the satellite x-axis direction, the spin axis, and its x-axis in the satellite z-axis direction, see Figure 2-1.

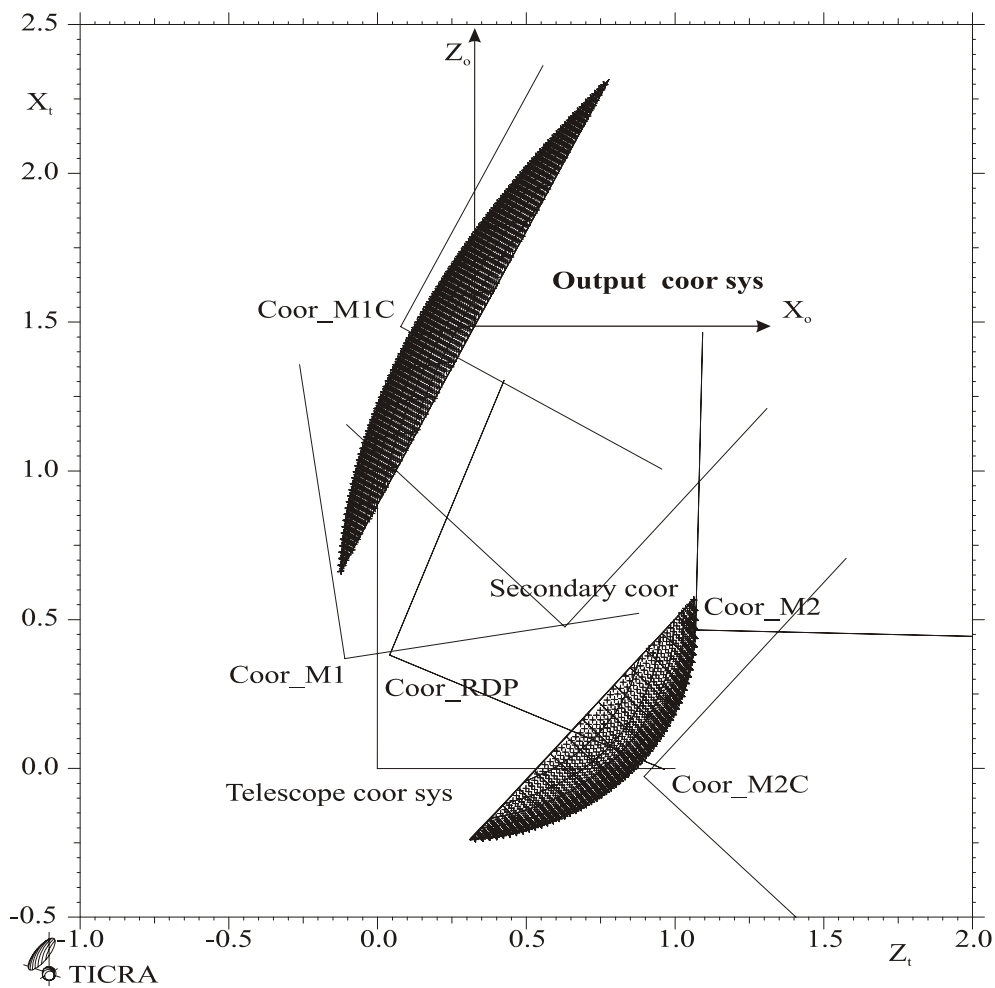


Figure 2-1 Output coordinate system.

The individual patterns are calculated in linear co and cx components in order to be able to superimpose them, but the main influence of the horn polarisation is removed by presenting the level of the field component along the major polarisation axis. The calculations are performed at 100 GHz using the HFI\_100\_1 detector horn.

The field around the main beam is shown in a raster plot in Figure 2-2. The main beam is located in the centre of the grid at  $\theta = 86.487^\circ$  and  $\phi = 1.183^\circ$  and the beam peak of 61.890 dBi is shown as a white spot. The colours give the levels of the field with a white maximum of 60 dBi and with colour shifts in 10 dB intervals down to -100 dBi. Everything below -100 dBi is black.

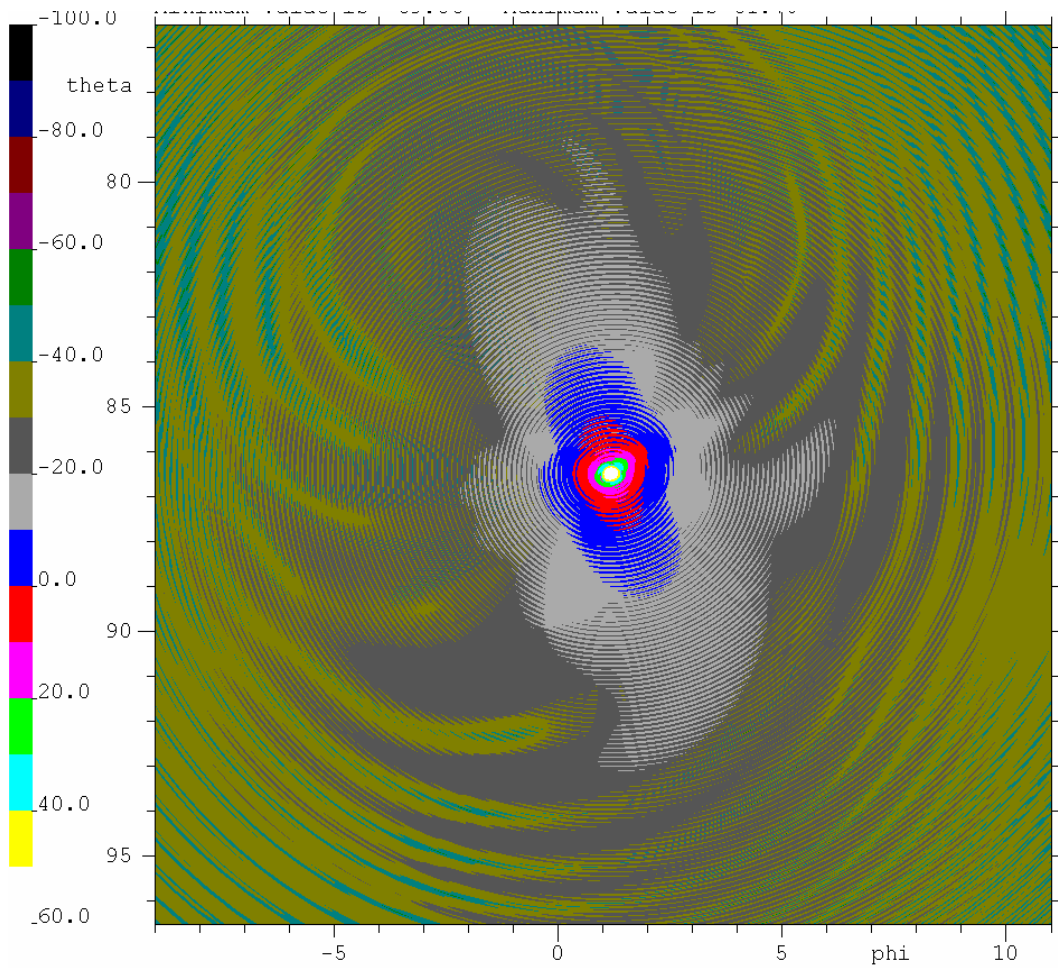


Figure 2-2 Far field from the PLANCK telescope with ideal mirrors.

### 3. MEASURED PRIMARY MIRROR

#### 3.1 Measured surface

The measured primary mirror surface data is delivered in the coordinate system M1, see Figure 3-1. The measurement is performed in a measurement coordinate system which is rotated  $-37.34465^\circ$  around the  $Y_{M1}$  axis, the M1C coordinate system. In this coordinate system the measurement points are placed in a nearly regular grid in the xy-plane with a distance of 20 mm and an accuracy of  $1 \mu$ . The 5702 xy-points are shown in Figure 3-2 in the RM1 coordinate system with the xy-plane parallel to the M1C coordinate system.. The delivered data was separated in two files. A file giving the measurement point in x and y and the z value of the geometrical best fit ellipsoid and a file containing the remaining  $\Delta z$  values. Therefore, these two data sets must first be added and then transposed to the primary mirror coordinate system (RM1), see Figure 3-1.

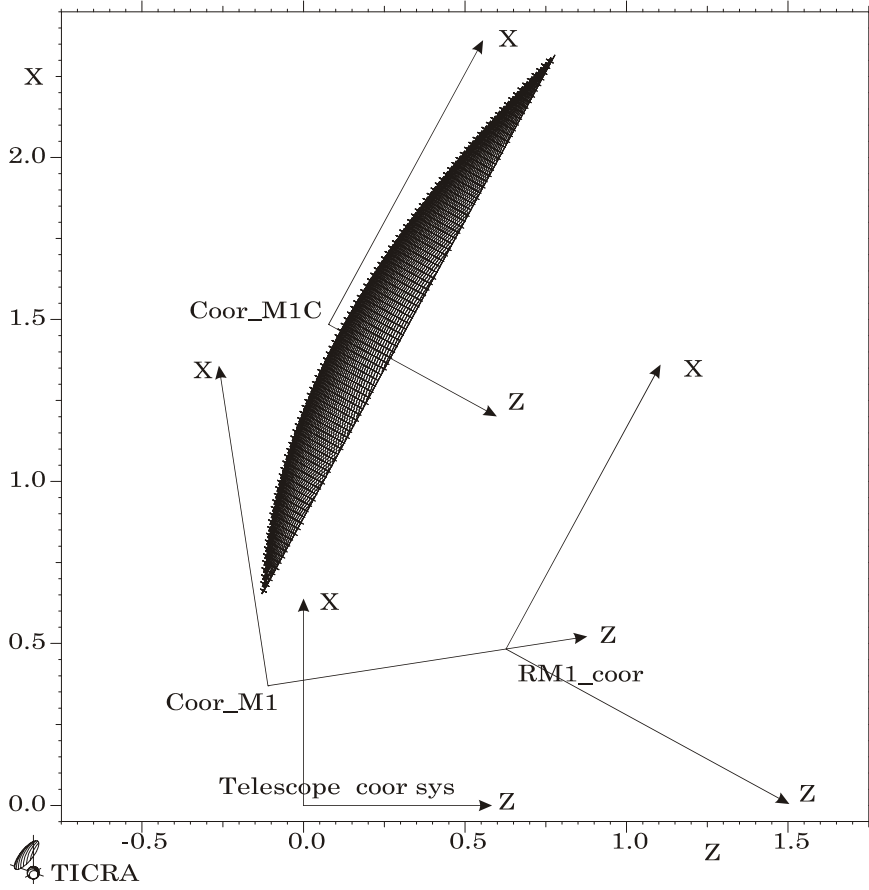


Figure 3-1 Primary mirror

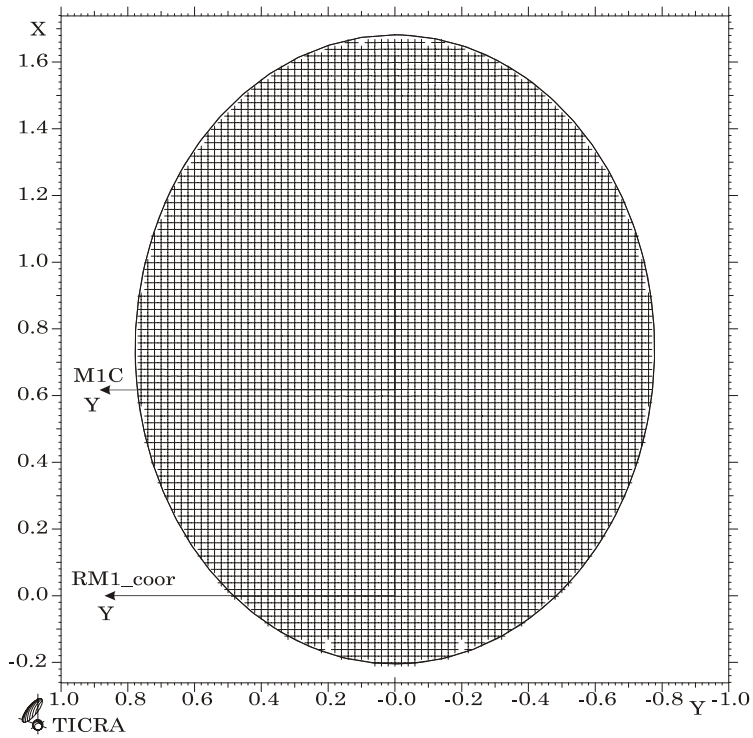


Figure 3-2 Measured points in xy-plane in RM1 coor. Sys.

The surface degradation is found by subtraction of the nominal mirror surface, see Figure 3-3.

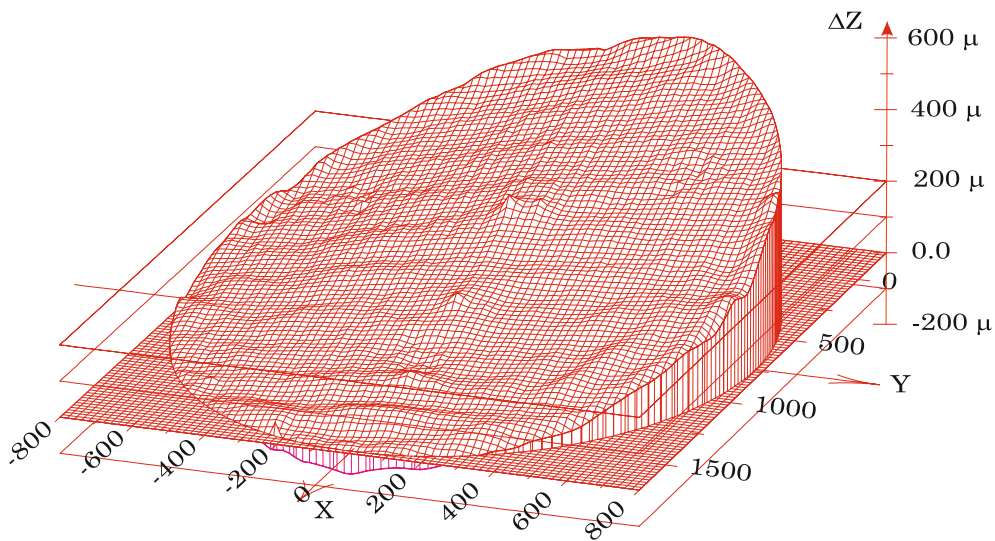


Figure 3-3 Total surface degradation

The distorted surface has an average of  $199.5 \mu$  and a tilt in the  $xz$ -plane and in the  $yz$ -plane of  $-0.0160^\circ$  and  $0.0093^\circ$ , respectively.

The best fit ellipsoid is defined by

$$r = -1440.085 \text{ and } K = -.869396$$

giving the following GRASP parameters

$$\begin{aligned} \text{focal distance} &= 20,562.24 \text{ mm} \\ \text{vertex distance} &= 22,052.69 \text{ mm} \end{aligned}$$

The remaining surface degradation is found by subtraction of this geometrical best fit ellipsoid, see Figure 3-4.

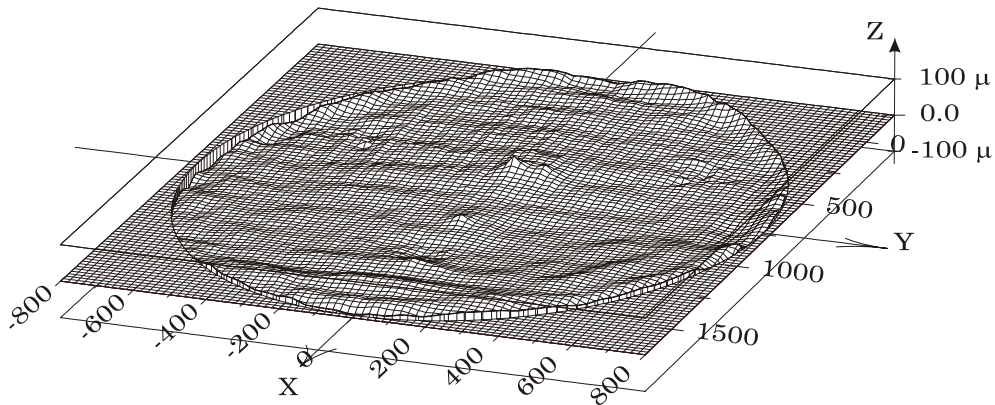


Figure 3-4 Remaining surface degradations

The distorted surface has an average of  $-3 \mu$ , a remaining overall rms of  $13 \mu$ , a maximum of  $51 \mu$  and a minimum of  $-42 \mu$ .

The distorted surface is also shown in Figure 3-5 as a contour plot with a contour line distance of  $1 \mu$ .

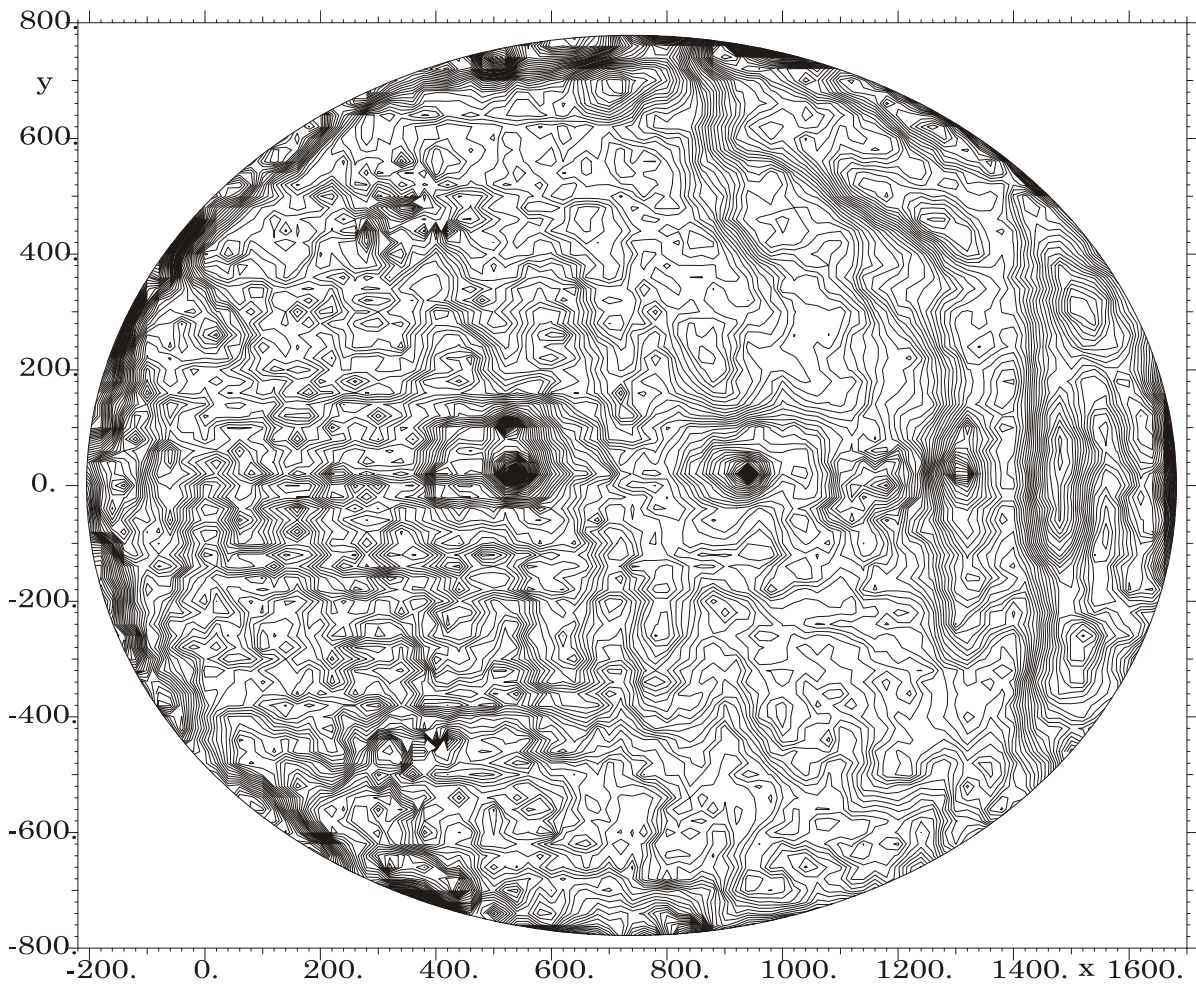


Figure 3-5 Remaining surface degradations with  $1 \mu$  intervals.

### 3.2 RF performance

The RF effects of the primary mirror surface degradations are presented in the same  $\phi$ - $\theta$  grid as for the nominal mirror system in Section 2, and the field around the main beam is shown in a raster plot in Figure 3-6. The main beam is located in the centre of the grid at  $\theta = 86.486^\circ$  and  $\phi = 1.184^\circ$ . Due to the aperture degradation the beam tilt is then  $\Delta\theta = -0.001^\circ$  and  $\Delta\phi = 0.001^\circ$ , and the main beam peak is decreased by 0.006 dB to 61.884 dBi.

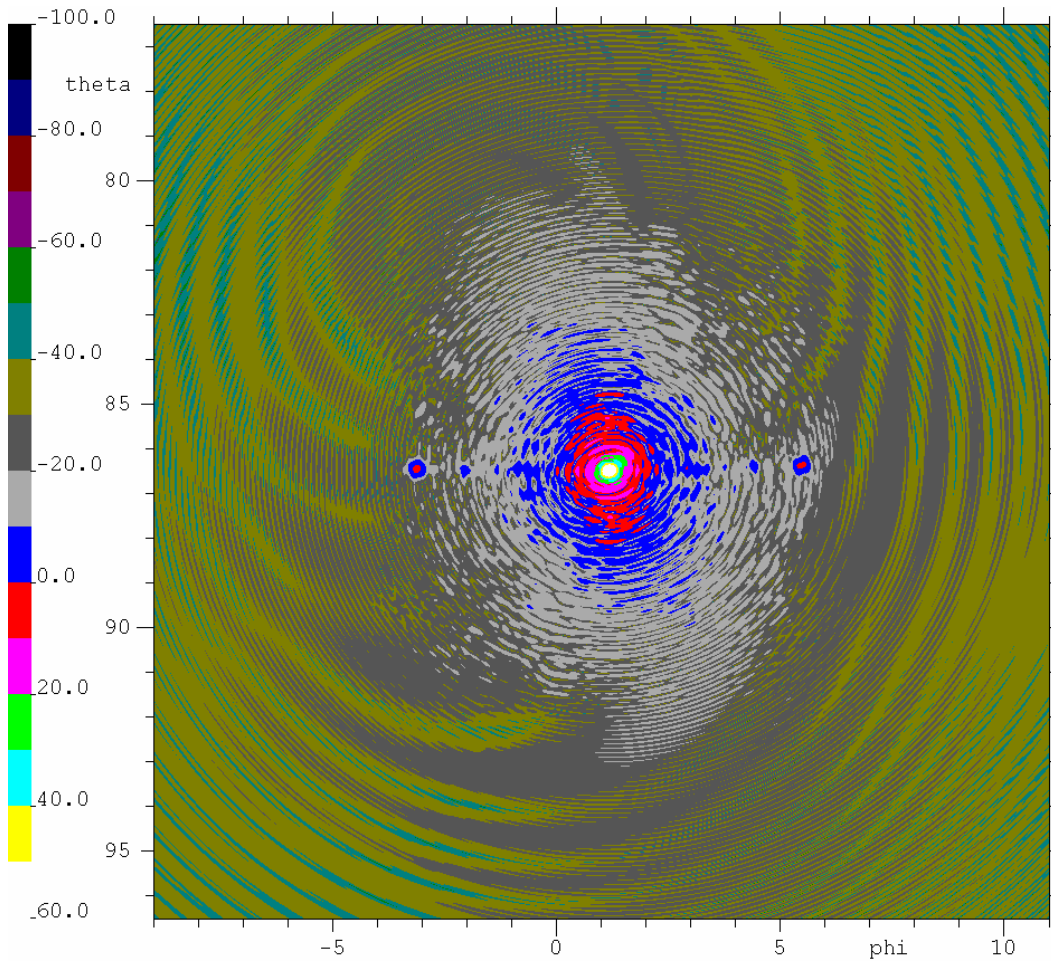


Figure 3-6 Far field from the PLANCK telescope with measured primary mirror surface.

The pattern shows large grating lobes near the conical  $\theta = 86.5^\circ$  cut. A pattern cut through these lobes is shown in Figure 3-7

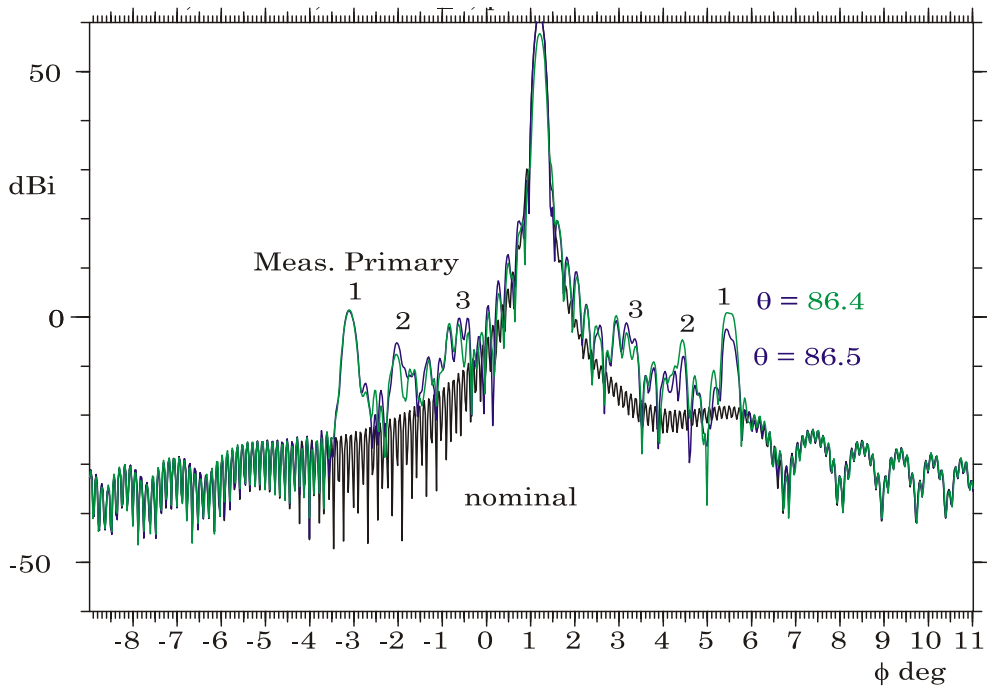


Figure 3-7 Pattern cut for  $\theta = 86.4^\circ$  .

The grating lobes are characterised by a shape like the main beam but in an angular distance,  $\Delta\theta$ , from the main beam and symmetric around the main beam. The interval length,  $s$ , of the associated regular distortions in the aperture is found by:

$$s = \lambda / \sin(\Delta\theta)$$

The largest grating lobes are found for  $\phi = -3.1^\circ$  and  $\phi = 5.5^\circ$  with peaks of 1.9 dB and 1.1 dB, respectively. The special distance from the main beam is  $4.3^\circ$ , which corresponds to a regular surface degradation with 40 mm spacing in the y-direction. The regularity is easy to recognize on the surface contour curves in Figure 3-5. The most likely explanation for this error is the measurement procedure itself. The measurement is performed in scans starting at the rim and measuring for nearly constant y value from the maximum x-value to the minimum x-value. After one scan the probe is moved to the next y-value and the scan is now performed in the opposite direction from the minimum x-value to the maximum x-value. This may create different measurement errors for each scan. The scans are performed with 20 mm spacing, giving similar errors with 40 mm spacing in the y-direction. In order to minimize a measurement error like this a so-called tie scan may be performed through the centre of the mirror and for constant x value. All scans may then be corrected by adjustment to these values.

In order to use the present surface data the measurement error may also be corrected by introducing a surface grid with the negated measurement error data or by changing the measurement data directly. The peak error is estimated to be around  $\pm 1 \mu$ . The RF degradation with the above simulated surface error is shown in Figure 3-8. The grating lobes are seen to be exactly the same as in Figure 3-7. All other ripples are from the spherical aberrations in the nominal aplanatic system and due to the complex aperture illumination.

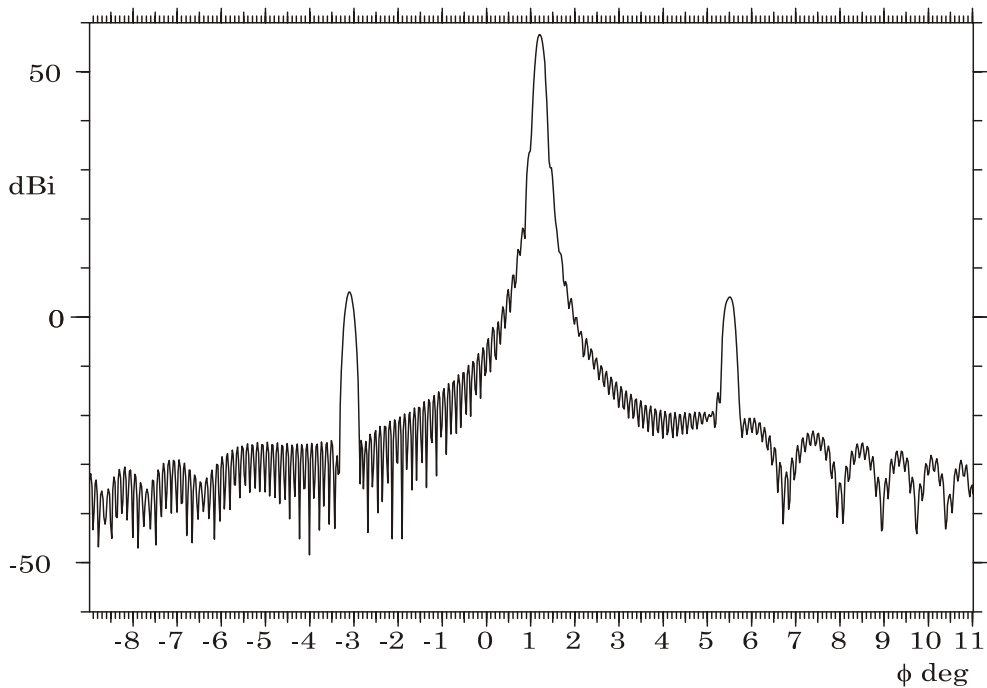


Figure 3-8 Pattern cut from regular measurement error for  $\theta = 86.4^\circ$ .

This distribution of the the surface measurement inaccuracy is the worst possible for the RF performance. Instead, if the  $\pm 1 \mu$  accuracy was distributed randomly, the RF distortion field was smoothen out over a wide angular region with a maximum peak level of -55 dBi.

The next grating lobes are found in Figure 3-7 for  $\phi = -2.1^\circ$  and  $\phi = 4.5^\circ$  with peaks of -5.1 dBi and -4.0 dBi, respectively. The special distance from the main beam is  $3.3^\circ$ , which associates to a regular surface degradation with 52 mm spacing in the y-direction. This corresponds very much to the distance between the centres of the hexagonal structure of the mirror honeycomb layer, see Figure 3-9.

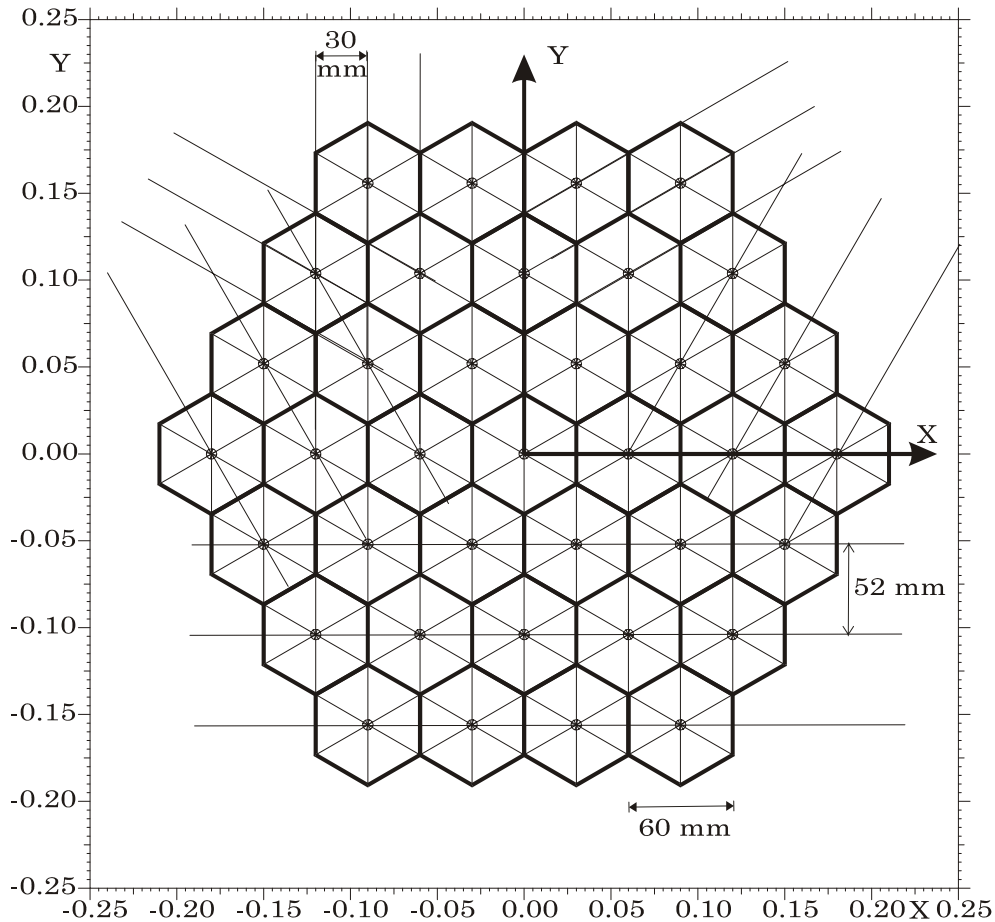


Figure 3-9 Hexagonal honeycomb structure.

In the y direction the distance is  $\sqrt{3} \cdot 30 \text{ mm} \approx 52 \text{ mm}$ . The lobe level indicates an average peak of the dimpling to be around  $1 \mu$  to  $2 \mu$ . The dimpling in the  $\pm 60^\circ$  direction may also create grating lobes in an angular distance of  $3.8^\circ$  from the main beam. The angle is larger than before due to a  $32.5^\circ$  tilt of the hexagonal supporting structure relative to the aperture in the main beam direction. The  $s = 30 \text{ mm}$  quilting rows will create grating lobes in the symmetry plane in an angular distance,  $\Delta\theta$ , given by:

$$\sin(\Delta\theta) = \lambda / (s \cdot \cos(32.5^\circ)) \Rightarrow \Delta\theta = 6.8^\circ$$

The quilting errors are simulated in GRASP using a new surface distortion object named "quilting\_surface", where the side length and the peak level is input. An enlarged single hexagonal section is shown in Figure 3-11. All 1<sup>st</sup> order derivatives are zero on the sides of the hexagon giving a smooth transition between the cells.

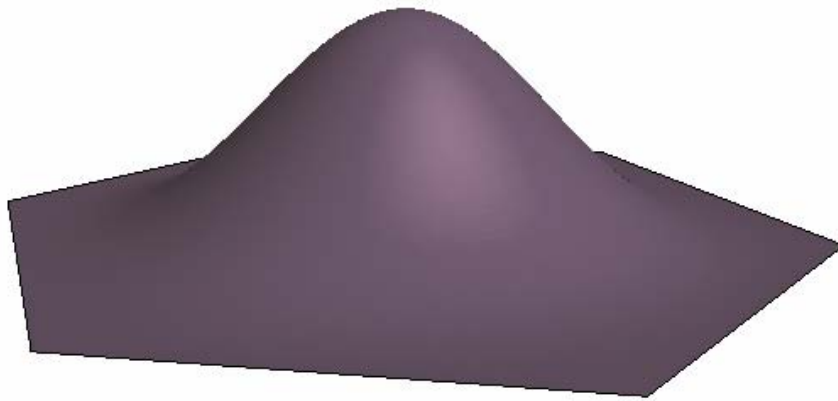


Figure 3-10 Simulated hexagonal honeycomb section.

Introducing this error with the dimensions of the present quilting structure and with a peak level of the dimpling of  $2\ \mu$  on the ideal primary mirror the RF performance is degraded as in Figure 3-11.

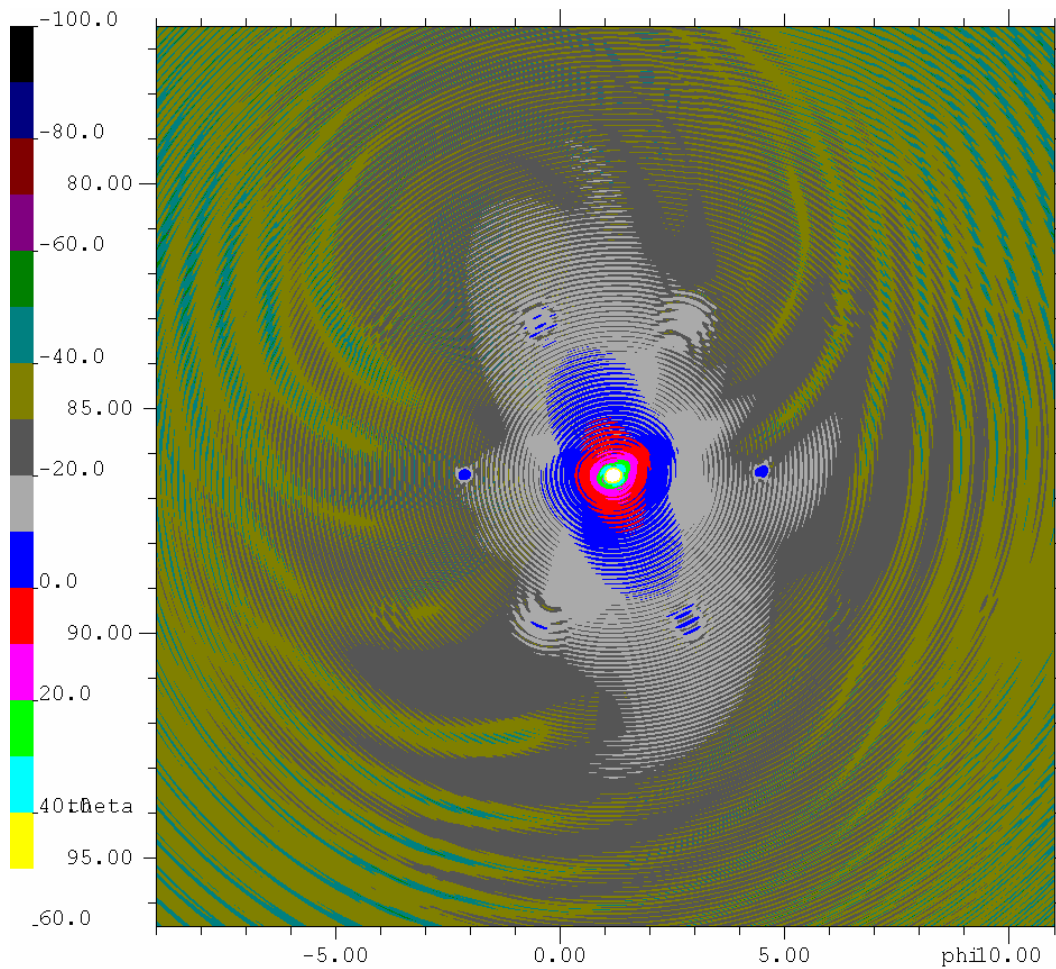


Figure 3-11 Far field from the PLANCK telescope with quilting errors on the primary mirror surface.

The grating lobes are clearly seen in the asymmetry plane and in the  $\pm 60^\circ$  direction. The lobes in the asymmetry plane is also shown in Figure 3-12, where the peaks are found for  $\phi = -2.1^\circ$  and  $\phi = 4.5^\circ$  with levels of -1.3 dBi and -1.0 dBi, respectively. The positions are the same as in Figure 3-7, but the levels are 1.7 dB larger. Therefore, the average quilting peak of the measured primary surface must be around  $1.6 \mu$

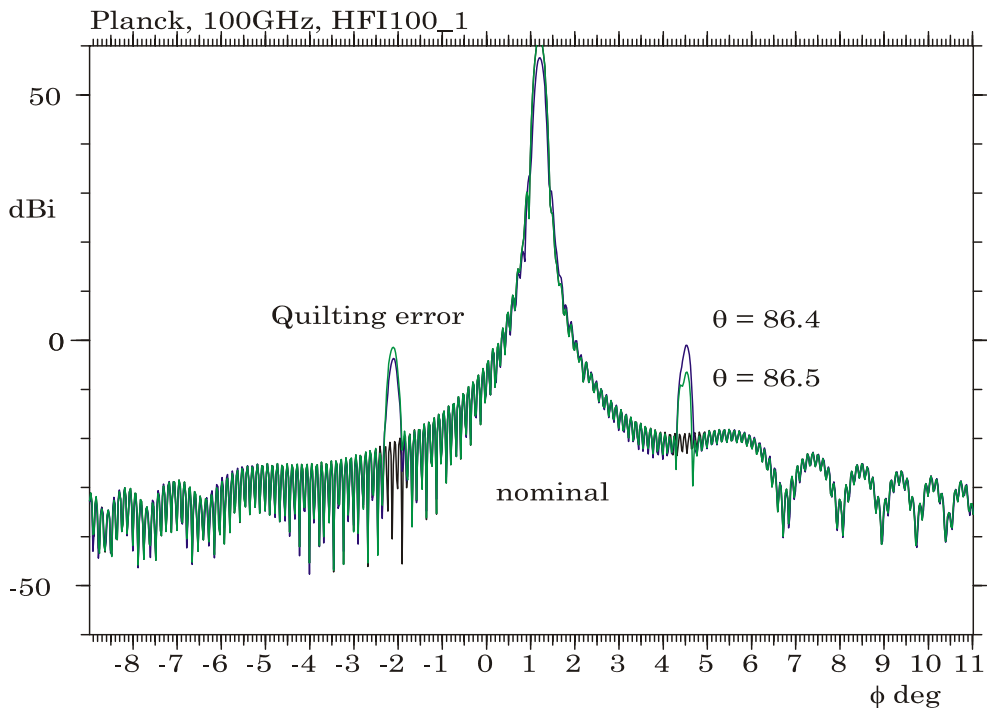


Figure 3-12 Quilting error in asymmetry plane for  $\theta = 86.4^\circ$  and  $\theta = 86.5^\circ$ .

The other simulated grating lobes are more evident in the difference pattern shown in Figure 3-13, where the nominal pattern from Figure 2-2 is subtracted.

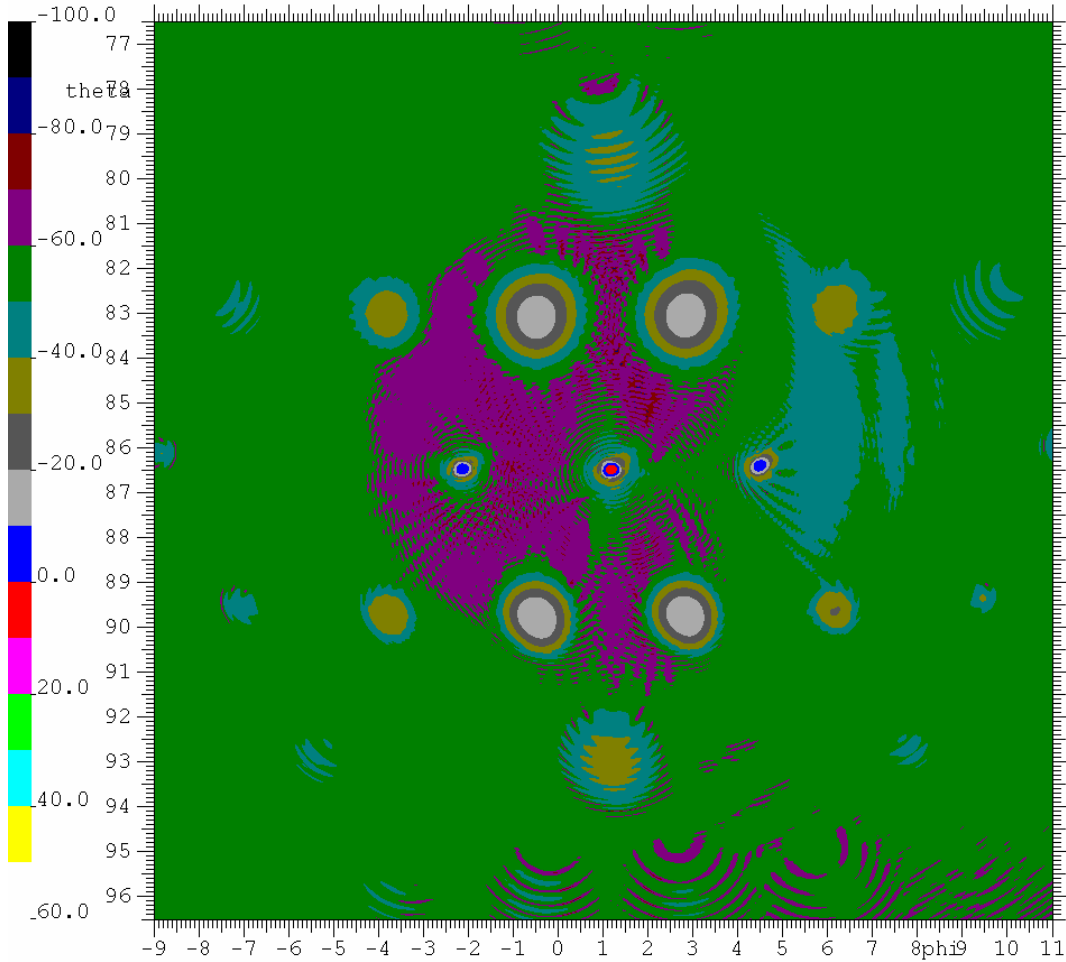


Figure 3-13 Difference field from the PLANCK telescope with quilting errors on the primary mirror surface.

The grating lobes out of asymmetry plane are smeared out due to the offset of the primary mirror giving slightly different hexagon distance in the upper and lower part. Nevertheless, the lobes near main beam may be identified in the difference pattern shown in Figure 3-14, where the nominal pattern from Figure 2-2 is subtracted from the distorted pattern in Figure 3-6.

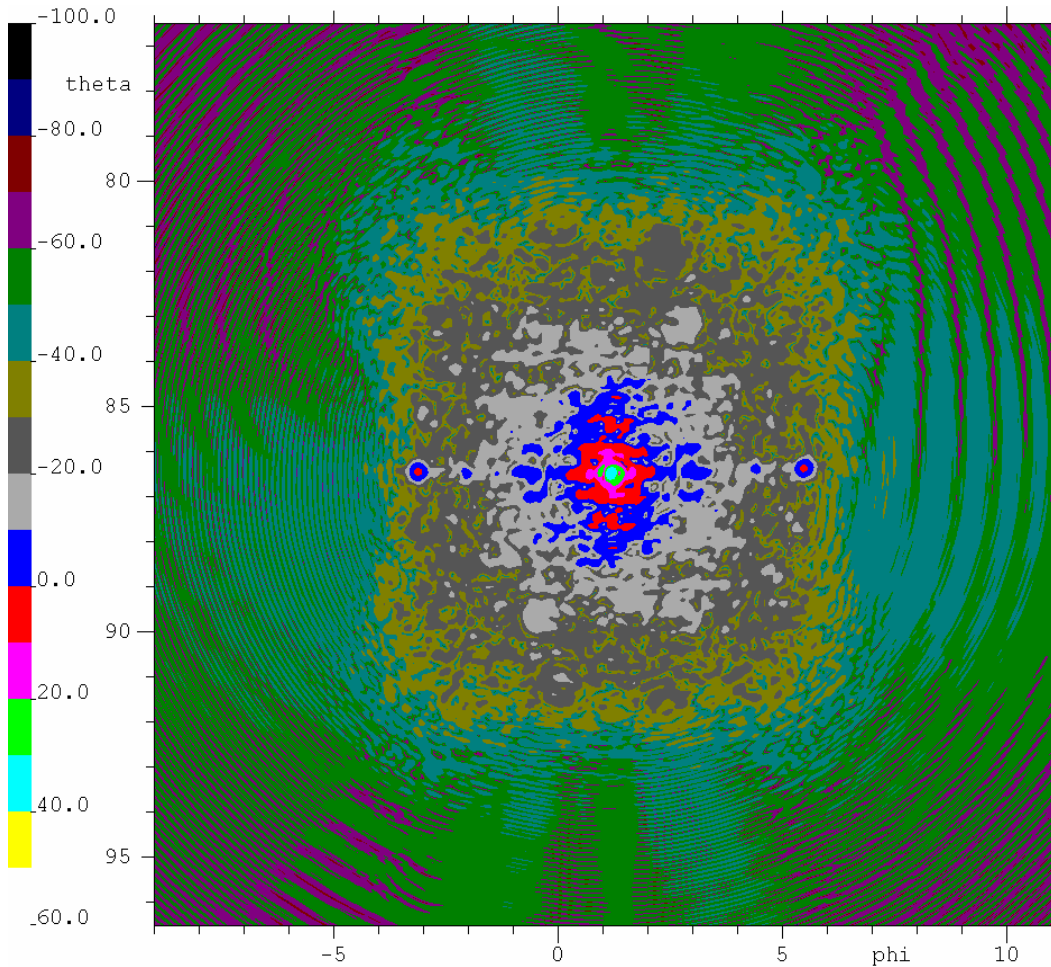


Figure 3-14 Difference field from the PLANCK telescope with measured primary mirror surface.

The pattern is only changed inside an angular region of  $81.4^\circ < \theta < 91.6^\circ$  and  $-3.1^\circ < \phi < 5.5^\circ$ . Like in Fast Fourier Transform, FFT, this corresponds to an aperture grid with spacing distances in x and y of 17 mm and 20 mm, respectively.

$$\theta_{\max} = \arcsin(\lambda / (2\Delta))$$

where  $\Delta$  is either  $\Delta x$  or  $\Delta y$ .

Due to the offset of the primary mirror, the measurement spacing is reduced in the x direction of the aperture plane by approximately 0.8.

Therefore, the quilting grating lobes outside this region can only be calculated if the surface is measured with a finer spacing.

The directions of the grating lobes are given in the following table.

$\phi_{xy}$ angle	Grid spacing	Grating lobe, $\Delta\theta$ , from
-------------------	--------------	-------------------------------------

[degrees]	s	Grid spacing	RF performance
0°, 180°	30mm*0.84≈25mm	≈6.8°	
±30°,±150°	52mm*0.87≈45mm	≈3.8°, ≈7.6°	3.6°
±60°,±120°	30mm*0.96≈29mm	≈6.0°	
±90°	52mm	≈3.3°, ≈6.6°, ≈10.0°	3.3°

The lobes near the main beam marked by index 3 in Figure 3-7 are created by the two centre surface distortion spots near  $(x,y) = (540 \text{ mm}, 20 \text{ mm})$  and  $(x,y) = (520 \text{ mm}, 100 \text{ mm})$ , see Figure 3-5. The two distortions are simulated by two Gaussian hats with peaks of  $64 \mu$  and  $39 \mu$  on the ideal primary mirror surface and the RF performance from these directions is calculated and shown in Figure 3-15. The lobes conform very much to the measured pattern.

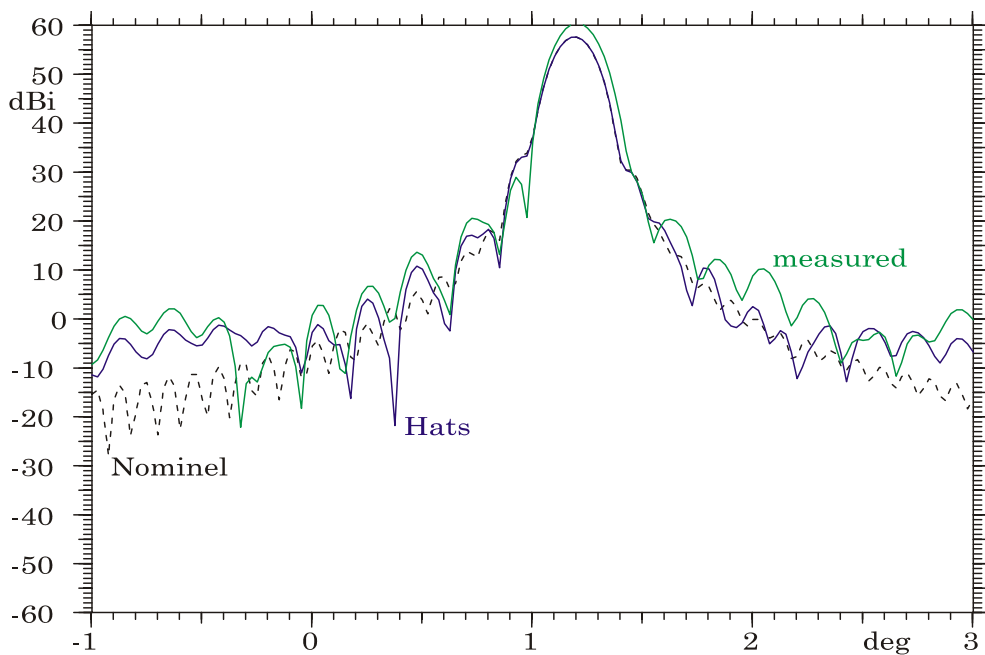


Figure 3-15 Pattern cut for  $\theta = 86.4^\circ$ .

The lobes in the symmetry plane are also created by these spots but together with the distortion spot near  $(x,y) = (940 \text{ mm}, 0 \text{ mm})$ , see Figure 3-16. The pattern from this spot simulated by a Gaussian hat with a peak of  $41 \mu$  is shown in Figure 3-17.

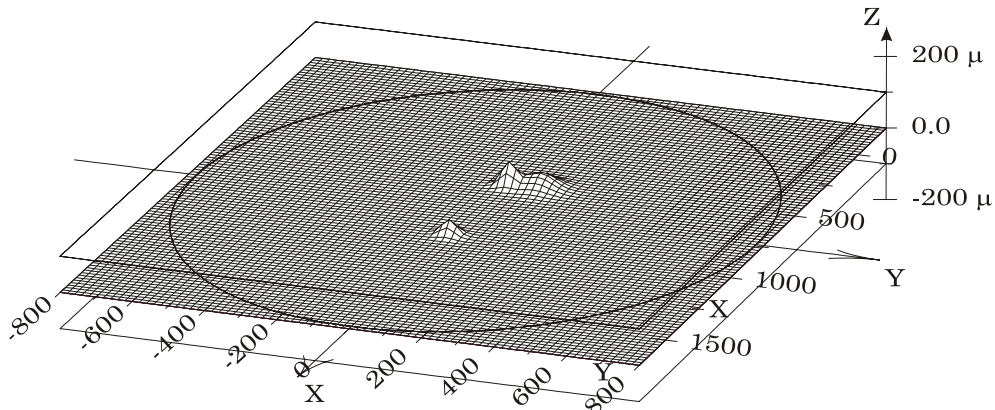
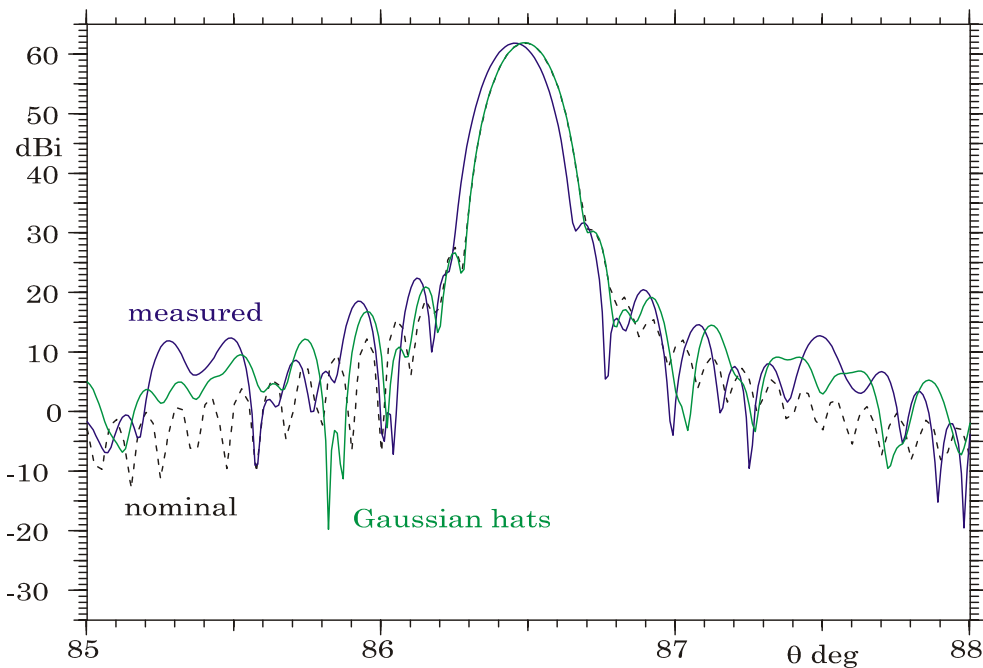


Figure 3-16 Gaussian hats

Figure 3-17 Pattern cut for  $\phi = 1.1831^\circ$ .

The lobes near  $\theta = 85.3^\circ$  are generated by the periodic distortion in the x direction, see Figure 3-18, with a periodicity of 160 mm and a peak near the edges of  $\pm 5 \mu$ . By introducing this periodic error as a cosine distortion on the nominal primary surface the RF performance is degraded as shown in Figure 3-19. The grating lobes are positioned near the  $\theta = 85.2^\circ$  and the  $\theta = 87.8^\circ$  direction with a field level of 18 dBi.

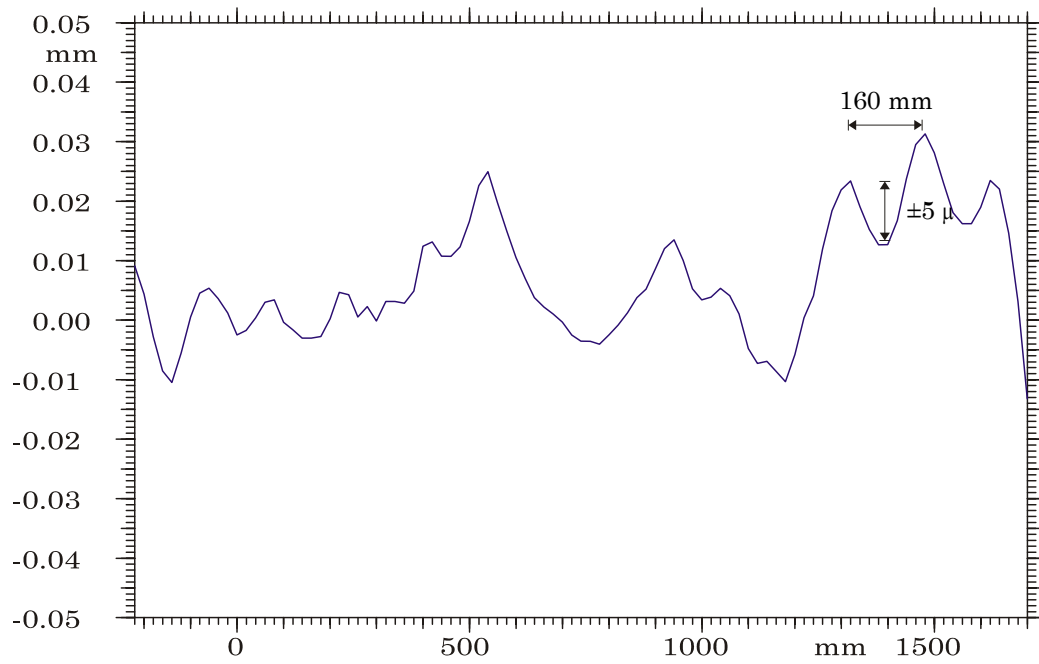


Figure 3-18 Measured surface distortions for  $y = 0$ .

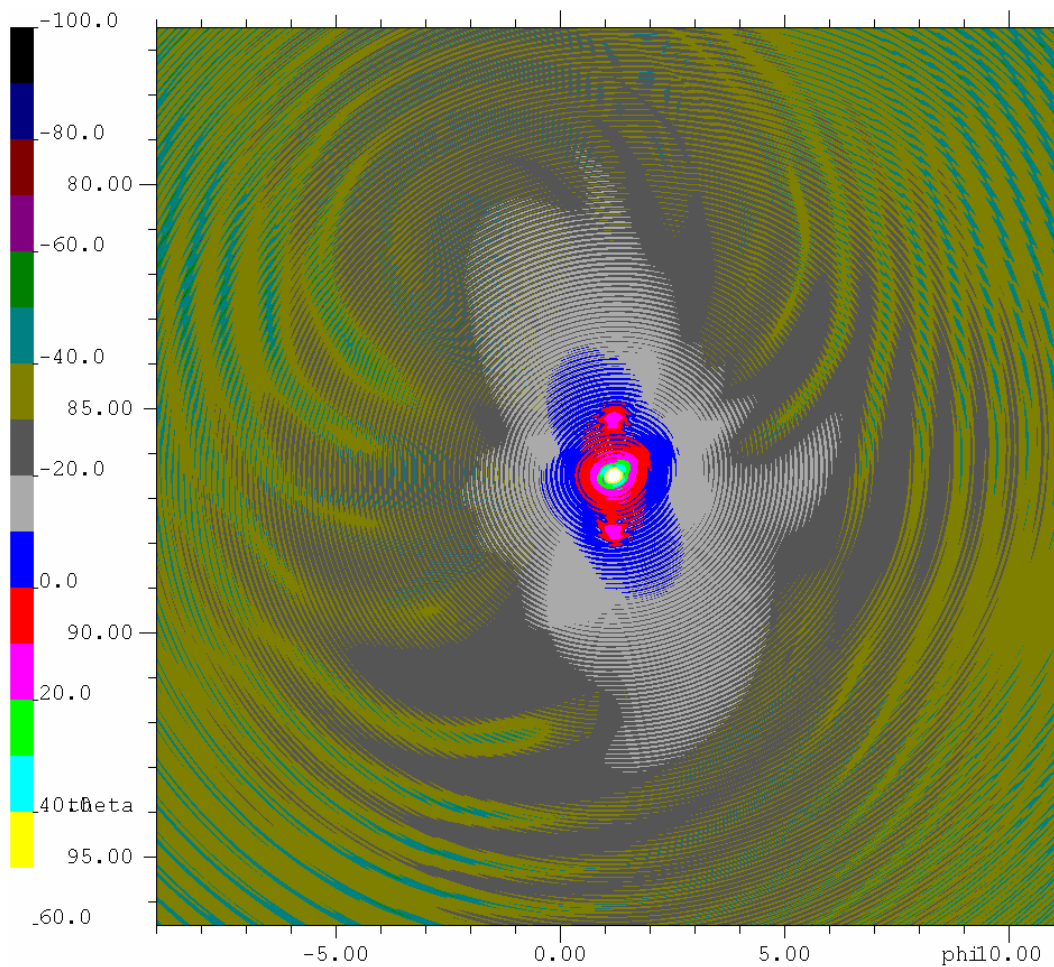


Figure 3-19 Field from the PLANCK telescope with periodic error on the primary mirror surface.

Figure 3-5 also shows three surface distortion spots near  $x = 400$  mm and  $y = \pm 500$  mm and in the symmetry plane for  $x \approx 1200$  mm. These spots may be generated by some kind of handle for the supporting booms. The size of the spots is approximated to a peak of  $10 \mu$  and a standard deviation of  $40$  mm. The Gaussian hats are shown in Figure 3-20. These spots will create lobes in the asymmetry plane with  $0.34^\circ$  spacing corresponding to the  $y$ -distance of the spots of  $500$  mm as seen in Figure 3-21 where the degradation field only is shown. The size of the distortions is seen to be too small to have any influence on the total pattern.

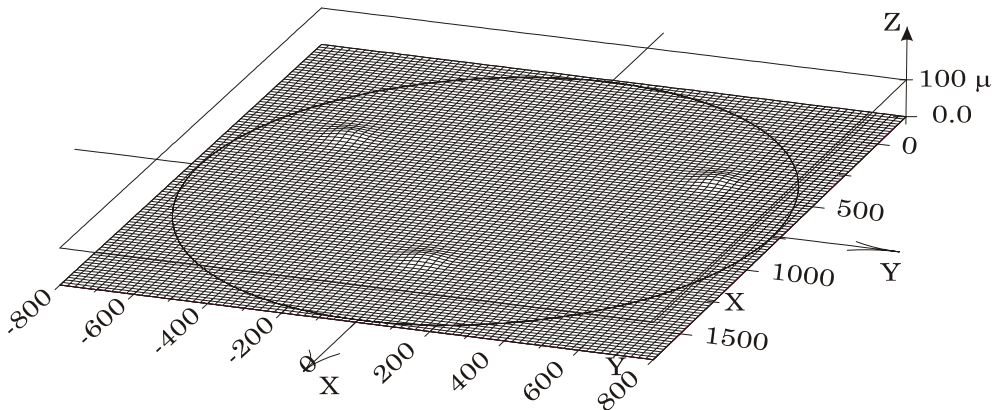


Figure 3-20 Gaussian hats simulating mirror support

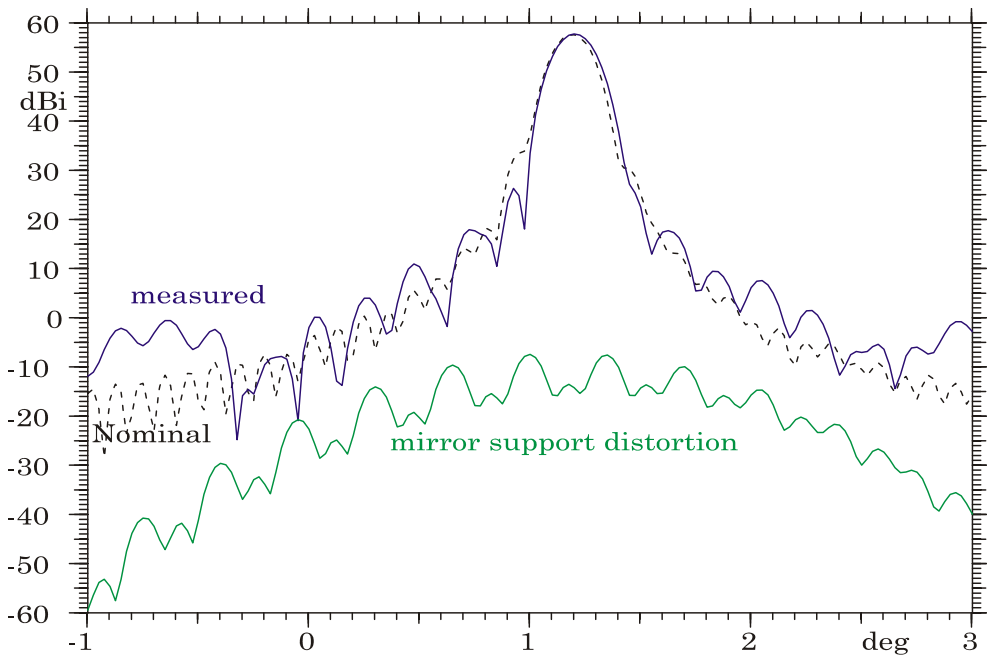


Figure 3-21 Pattern cut for  $\theta = 86.4^\circ$ .

## 4. MEASURED SECONDARY MIRROR

### 4.1 Measured surface

The measured secondary mirror surface data is delivered in the coordinate system M2, see Figure 4-1. The measurement is performed in a measurement coordinate system which is rotated  $41.443^\circ$  around the  $Y_{M2}$  axis, the M2C coordinate system. In this coordinate system the measurement points are placed in a nearly regular grid in the xy-plane with a distance of 10 mm and an accuracy of  $1\ \mu$ , see Figure 4-2. The delivered data was separated in two files. A file giving the measurement point in x and y and the z value of the geometrical best fit ellipsoid and a file containing the remaining  $\Delta z$  values. Therefore, these two data sets must first be added and then transposed to the secondary mirror coordinate system, see Figure 4-1.

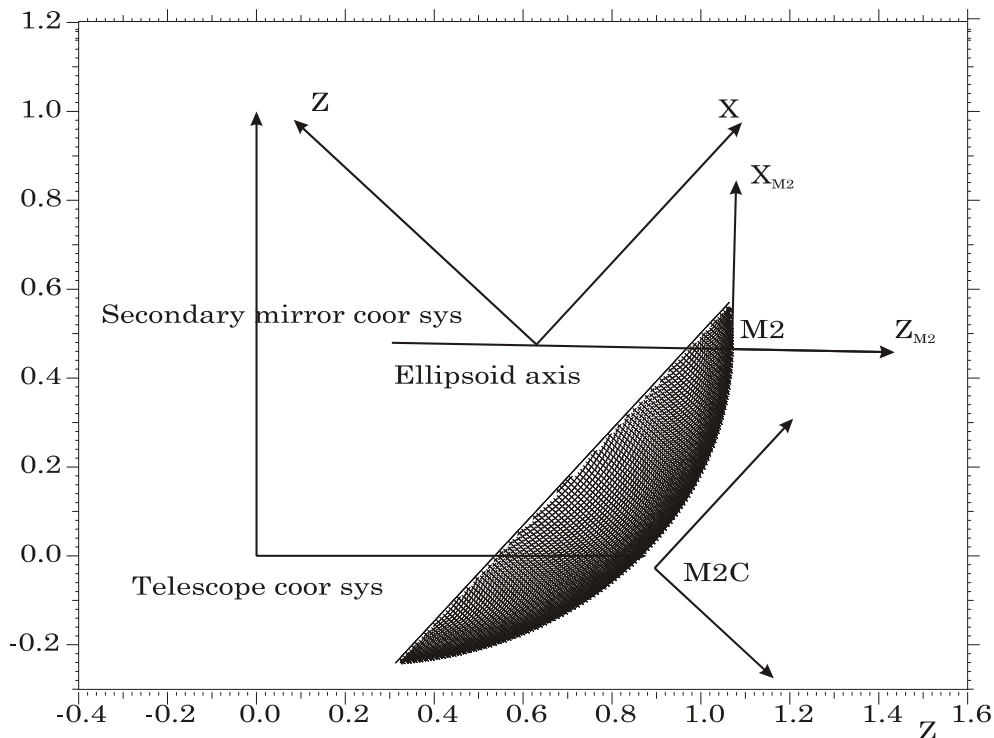


Figure 4-1 Secondary mirror

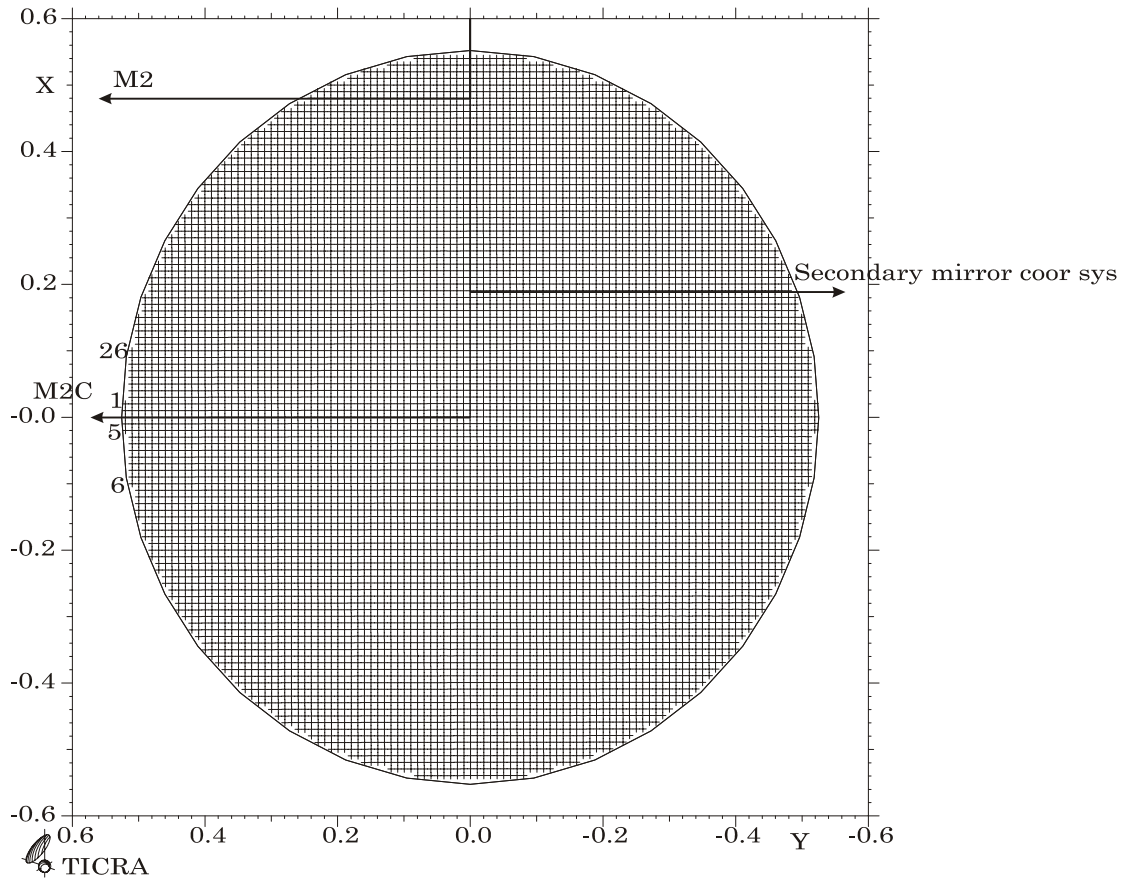


Figure 4-2 Measured points in xy-plane in Measurement coor. Sys, M2C.

The best fit ellipsoid is defined by

$$r = -644.043 \text{ and } K = -.215428$$

giving the following GRASP parameters

$$\begin{aligned} \text{focal distance} &= 762.0130533 \text{ mm} \\ \text{vertex distance} &= 1641.768186 \text{ mm} \end{aligned}$$

The remaining surface degradation is found by subtraction of this geometrical best fit ellipsoid, see Figure 4-3.

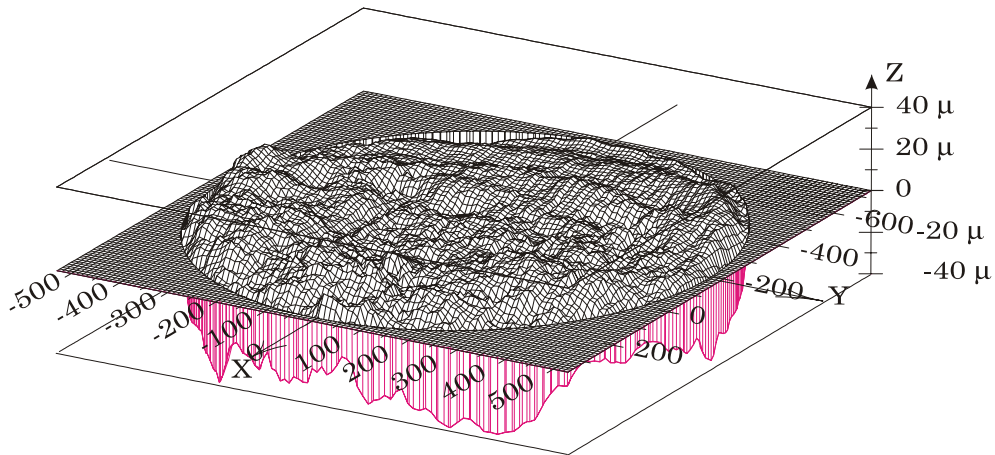


Figure 4-3 Surface degradation

The distorted secondary mirror surface has an average of  $-0.56 \mu$ , a remaining overall rms of  $9.2 \mu$ , a maximum of  $14 \mu$  and a minimum of  $-65 \mu$ .

The distorted surface is also shown in Figure 4-4 as a contour plot with contour line distance of  $1 \mu$ .

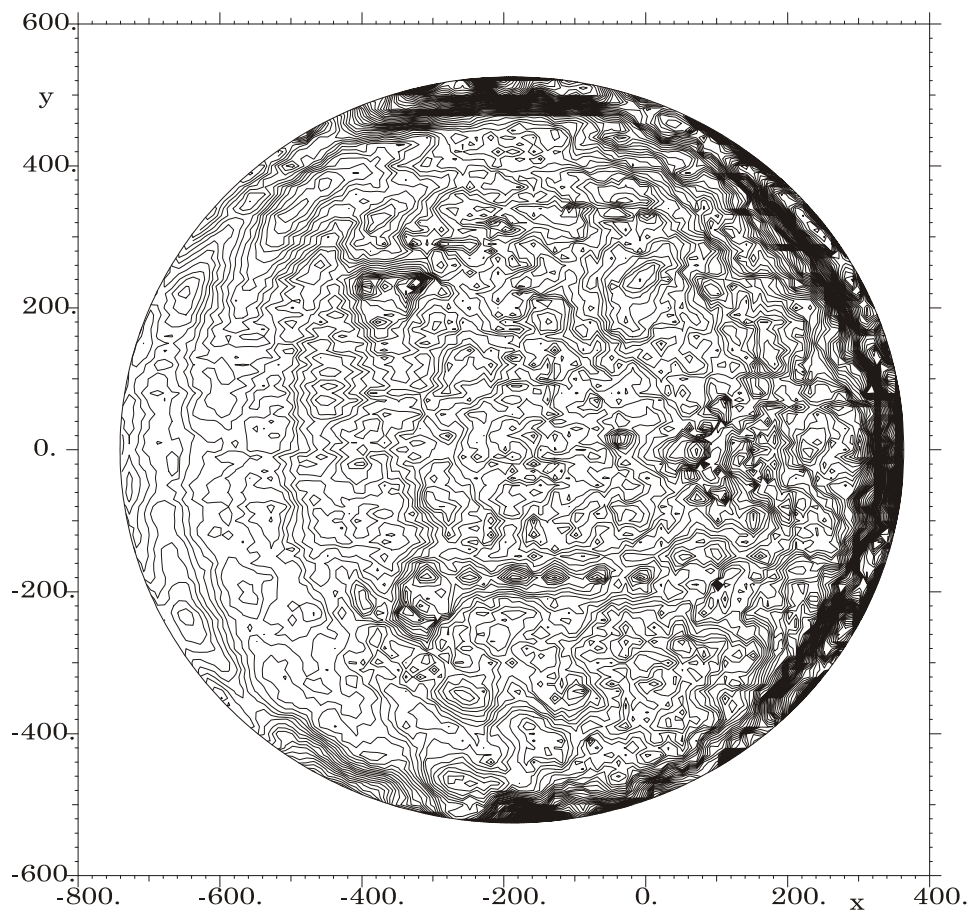


Figure 4-4 Remaining secondary mirror surface degradations with  $1 \mu$  intervals.

A quilting error is clearly seen in the x interval [-400 mm, 100 mm] in the  $y = -180$  mm plane. The distance between the peaks is exactly 60 mm as in the honeycomb spacing, see Figure 4-5, and the peaks are around  $6 \mu$  as seen in the cut for  $y = -180$  mm in Figure 4-6.

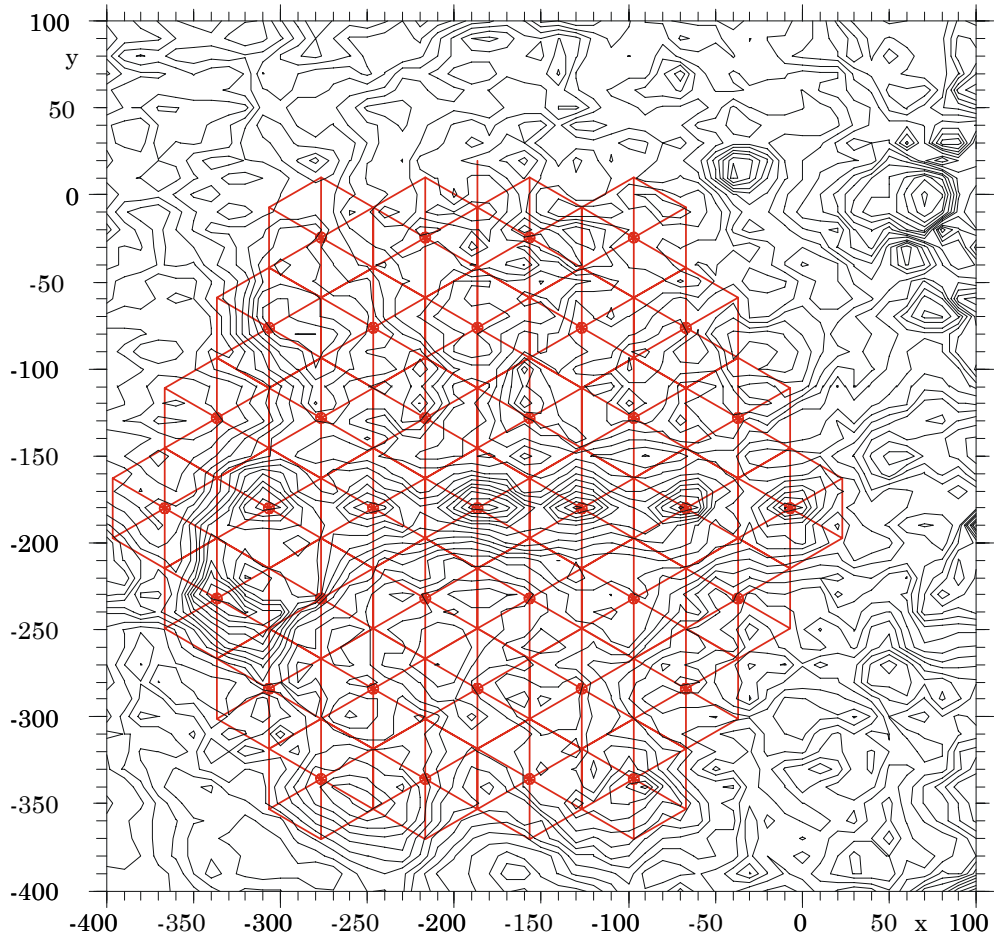


Figure 4-5 Remaining secondary mirror surface degradations with quilting grid.

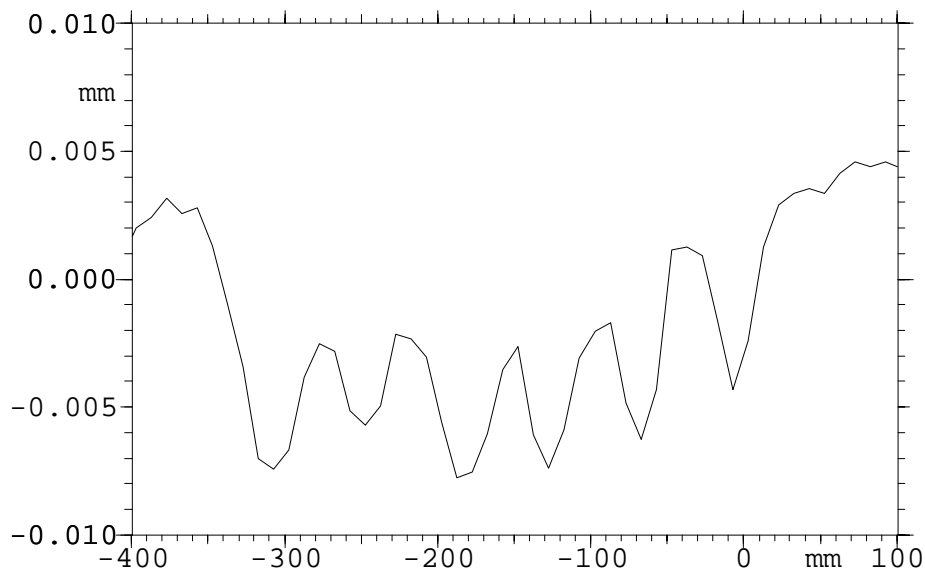


Figure 4-6 Remaining surface degradations in  $y = -180$  mm cut.

## 4.2 RF performance

The RF effects of the secondary mirror surface degradations are presented in the same  $\phi$ - $\theta$  grid as for the nominal mirror system in Section 2, and the field around the main beam is shown in a raster plot in Figure 4-7. The main beam is located in the centre of the grid at  $\theta = 86.484^\circ$  and  $\phi = 1.183^\circ$  and shown as a white spot. The colours give the levels of the field with a white maximum of 60 dBi and with colour shifts in 10 dB intervals down to -100 dBi. Everything below -100 dBi is black. Compared to the nominal field in Chapter 2 the aperture degradation gives a beam tilt of  $\Delta\theta = 0.003^\circ$  and  $\Delta\phi = 0.000^\circ$ , and the main beam peak is decreased by 0.009 dB to 61.881 dBi.

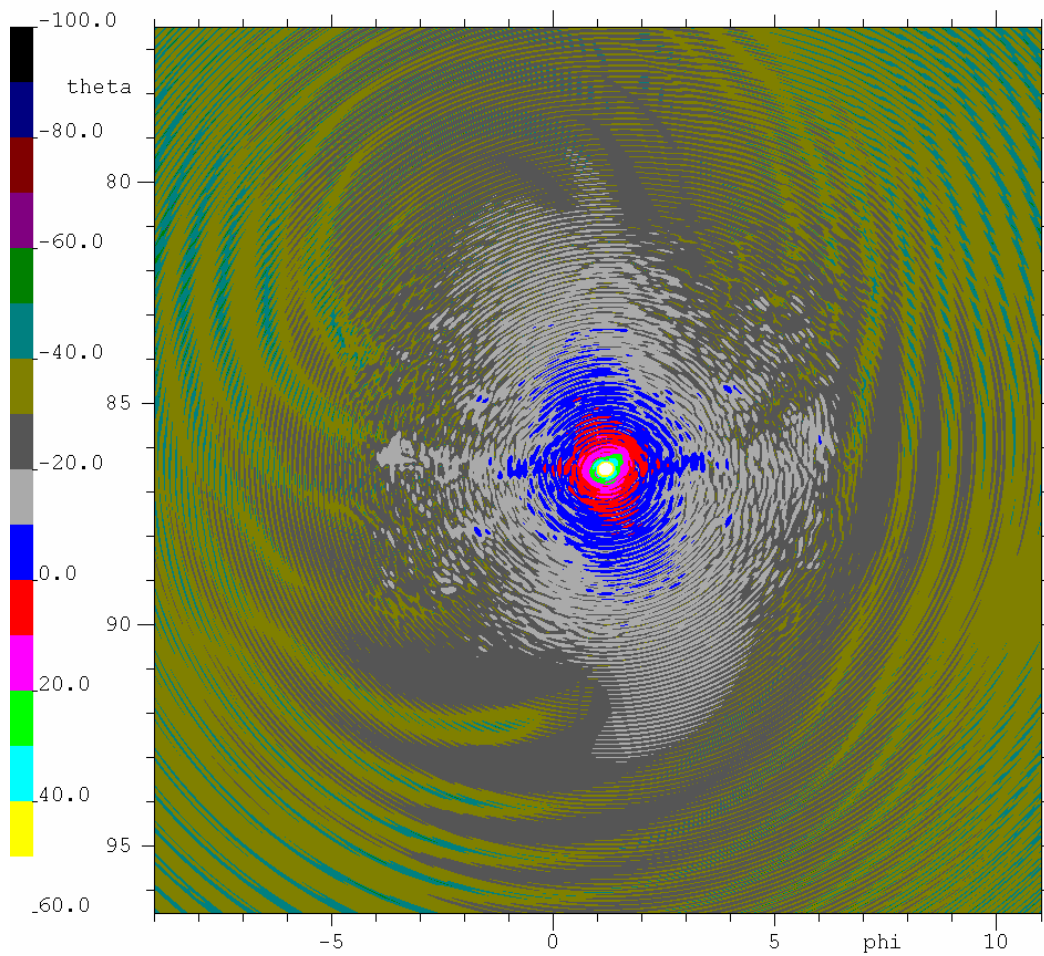


Figure 4-7 Far field from the PLANCK telescope with measured secondary mirror surface.

The changes of the pattern are more evident in the difference pattern shown in Figure 4-8, where the nominal pattern from Figure 2-2 is subtracted.

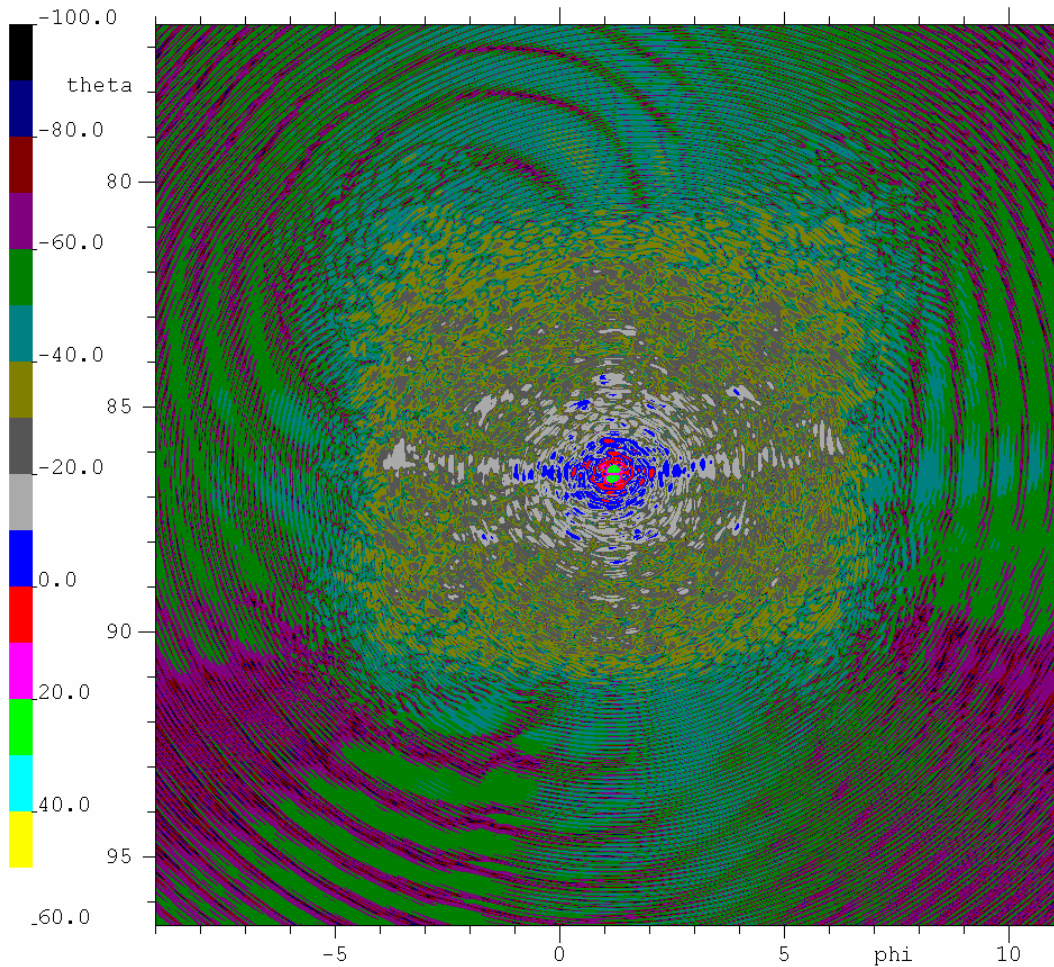


Figure 4-8 Difference field from the PLANCK telescope with measured secondary mirror surface.

The pattern is only changed inside an angular region of  $81^\circ < \theta < 91^\circ$  and  $-4^\circ < \phi < 7^\circ$ . Like in Fast Fourier Transform, FFT, this corresponds to an aperture grid with spacing distances in x and y of 18 mm and 17 mm, respectively.

$$\Delta x = .5 * \lambda / \sin(\theta_{\max})$$

Due to the geometry of the antenna, the measurement spacing of the secondary mirror is magnified in the aperture plane by approximately 1.9 and 1.7 in the x and y plane, respectively, see Figure 4-9

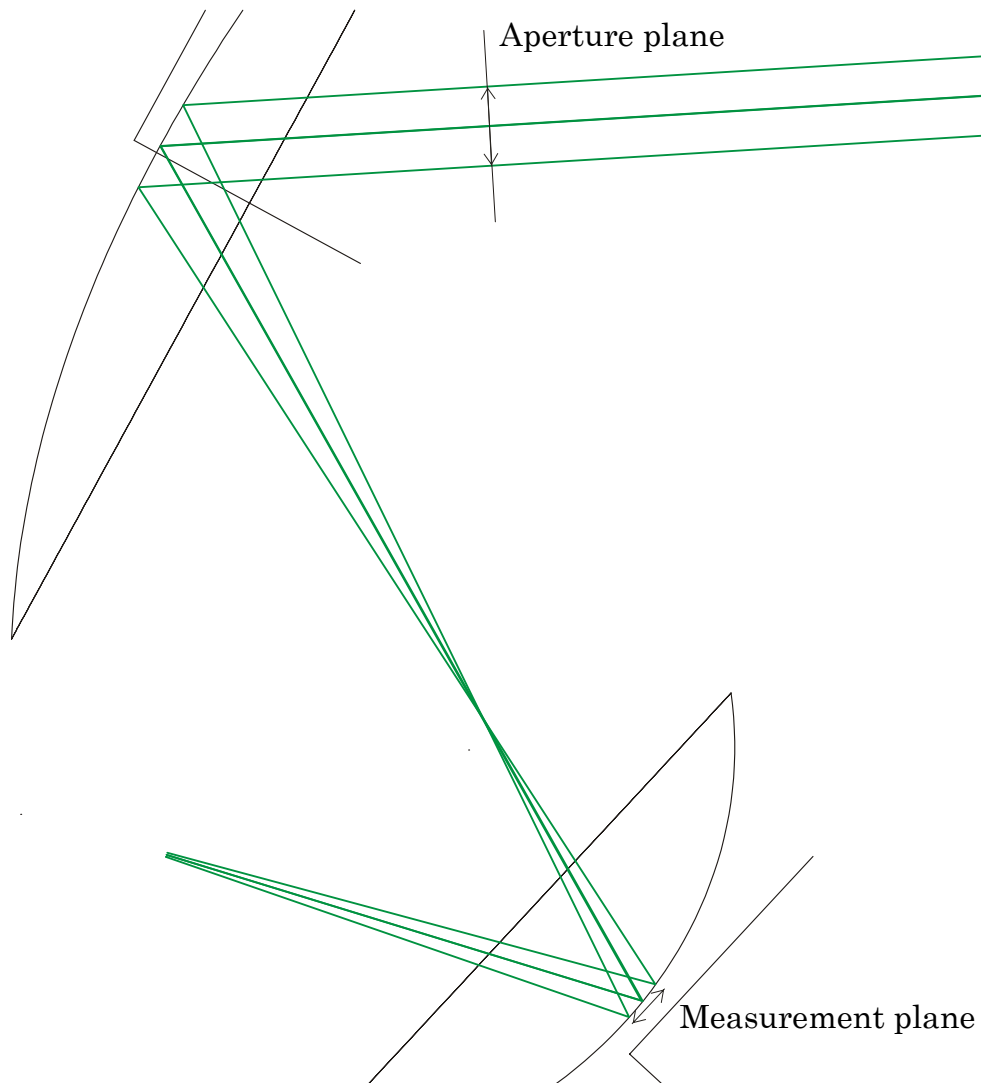


Figure 4-9 Mapping of measured secondary mirror surface grid to aperture plane.

The changed region is magnified in Figure 4-10, where new lobes are found in six planes around the main beam peak.

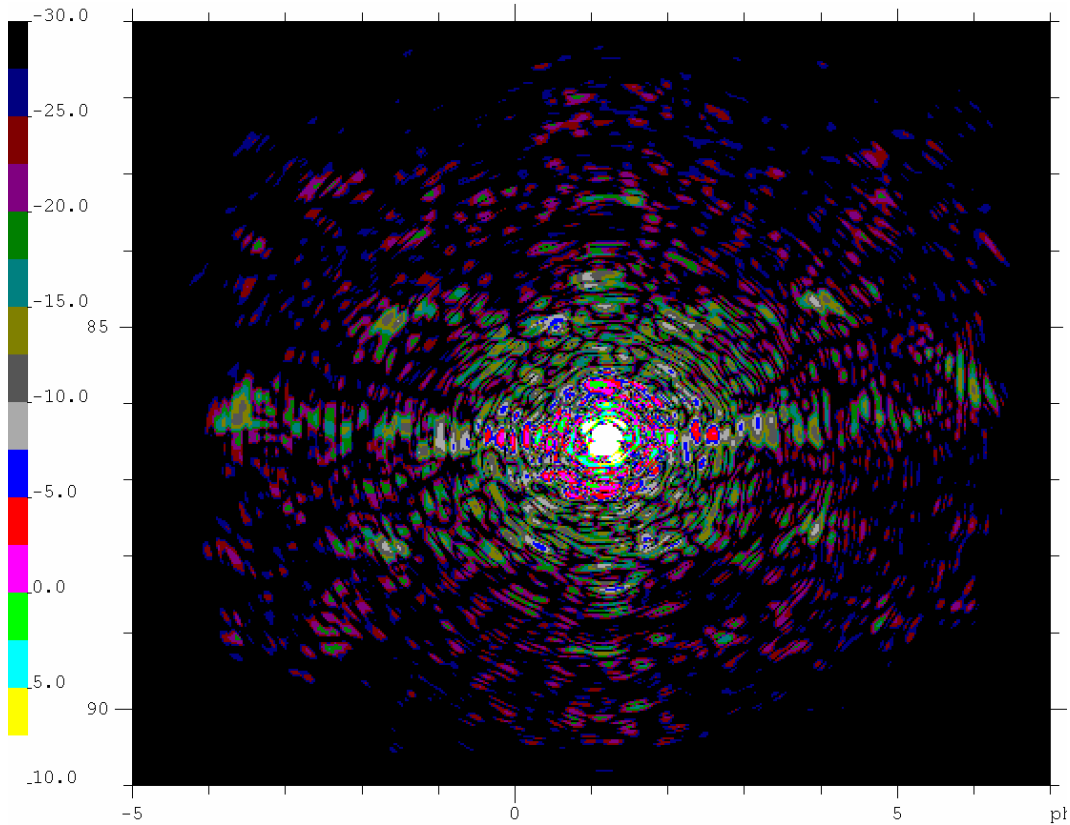


Figure 4-10 Far field from the PLANCK telescope with measured secondary mirror surface.

The two largest and most far out grating lobes are found for  $\phi = -3.7^\circ$  and  $\phi = 6.1^\circ$  with peaks around -10 dBi. The distance from the main beam is then  $4.9^\circ$ , which corresponds to a regular surface degradation with 20 mm spacing in the y-direction. The regularity is easy to recognize on the surface cut through the centre of the mirror with x constant -188.77 mm in Figure 4-11.

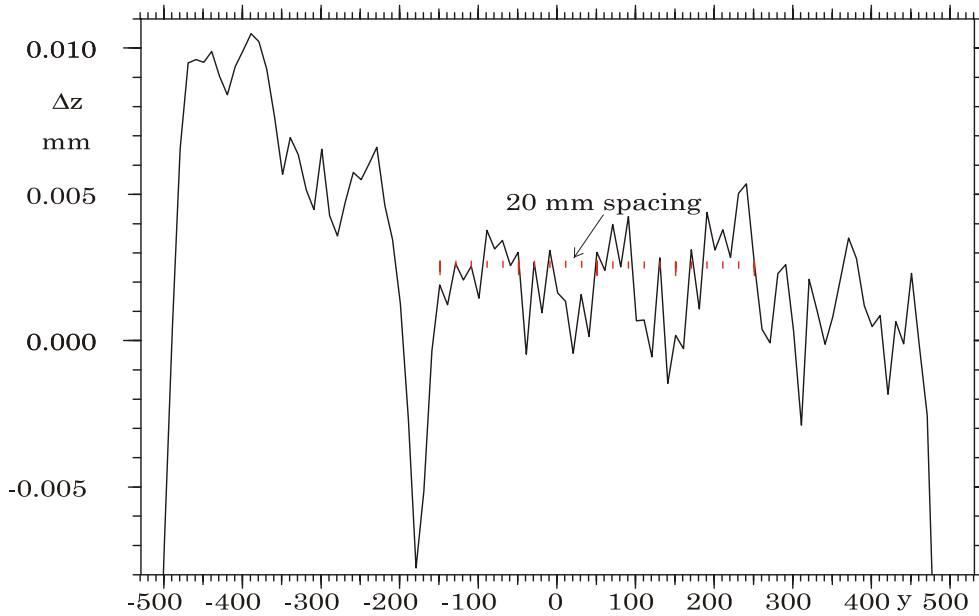


Figure 4-11 Far field from the PLANCK telescope with measured secondary mirror surface.

The most likely explanation for this error is the measurement procedure itself. The measurement is performed in scans starting at the rim and measuring for a nearly constant  $y$  value from the maximum  $x$ -value to the minimum  $x$ -value, see Figure 4-2 point 1 and 6, respectively. After one scan the probe is moved to the next  $y$ -value, point 6 in Figure 4-2, and the scan is now performed from the minimum  $x$ -value to the maximum  $x$ -value. This may create different measurement errors for each scan. The scans are performed with 10 mm spacing, giving similar errors with 20 mm spacing in the  $y$ -direction. The peak-to-peak error is estimated to be around  $0.7 \mu$ . The RF degradation with the above simulated surface error is shown in Figure 4-12. The grating lobes are seen to be exactly the same as in Figure 4-7. All other ripples are from the spherical aberrations in the nominal aplanatic system and due to the complex aperture illumination.

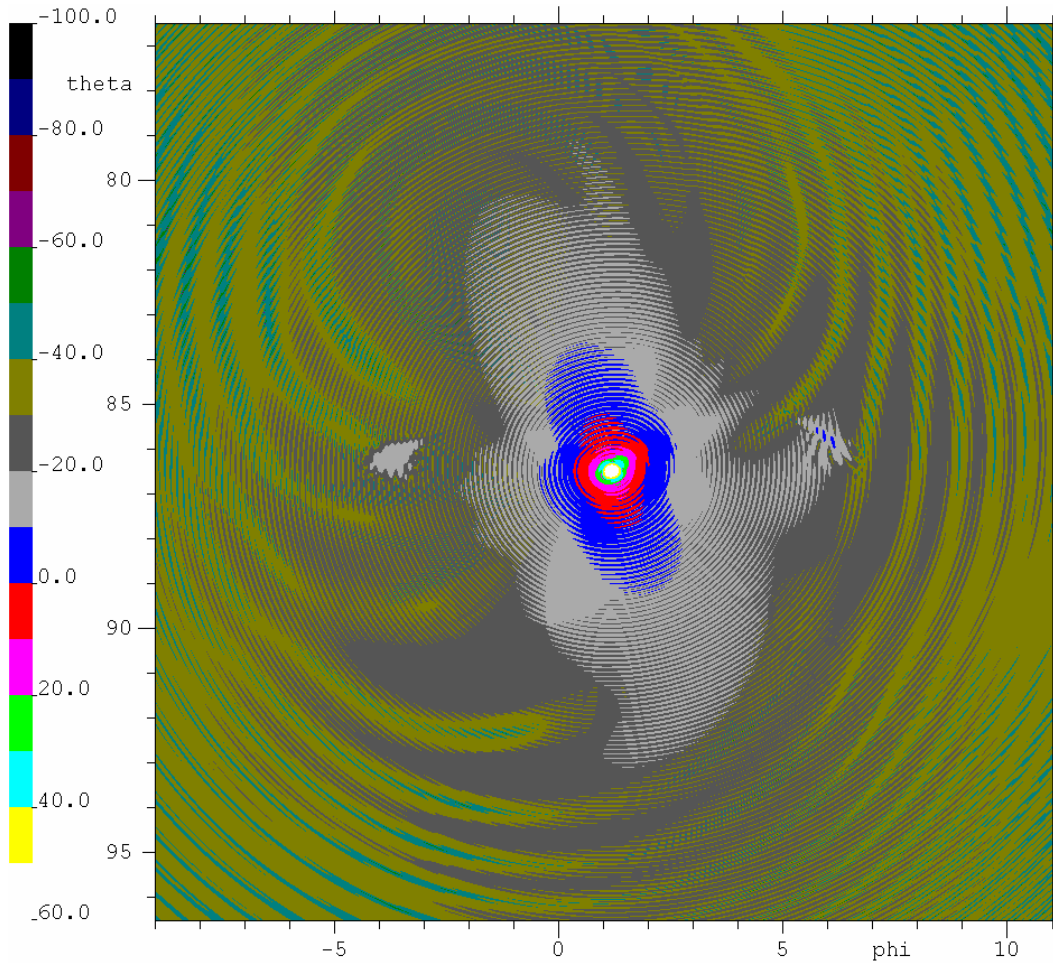


Figure 4-12 Far field from regular measurement error of secondary mirror surface.

The hexagonal structure of the mirror honeycomb layer, see Figure 4-5, may generate grating lobes in the following angular regions around the main beam. The grid distances are corrected with the projection factors in Figure 3-9.

$\phi_{xy}$ angle [degrees]	Grid spacing s	Grating lobe, $\Delta\theta$ , from	
		Grid spacing	RF performance
$0^\circ, 180^\circ$	30mm*1.9 $\approx$ 57mm	$\approx 3.0^\circ, \approx 6.0^\circ$	$2.9^\circ$
$\pm 30^\circ, \pm 150^\circ$	52mm*1.8 $\approx$ 94mm	$\approx 1.8^\circ, \approx 3.6^\circ, \approx 5.4^\circ$	$1.7^\circ, 3.6^\circ$
$\pm 60^\circ, \pm 120^\circ$	30mm*1.8 $\approx$ 54mm	$\approx 3.2^\circ, \approx 6.4^\circ$	$3.3^\circ$
$\pm 90^\circ$	52mm*1.7 $\approx$ 88mm	$\approx 1.9^\circ, \approx 3.8^\circ, \approx 5.7^\circ$	$2.0^\circ, 3.6^\circ$

The quilting errors are simulated in GRASP by superimposing this distortion on the ideal secondary mirror given the dimensions of the present quilting structure and with a peak level of the dimpling of  $6 \mu$  as found in Figure 4-5. The RF performance is degraded as in Figure 4-16.

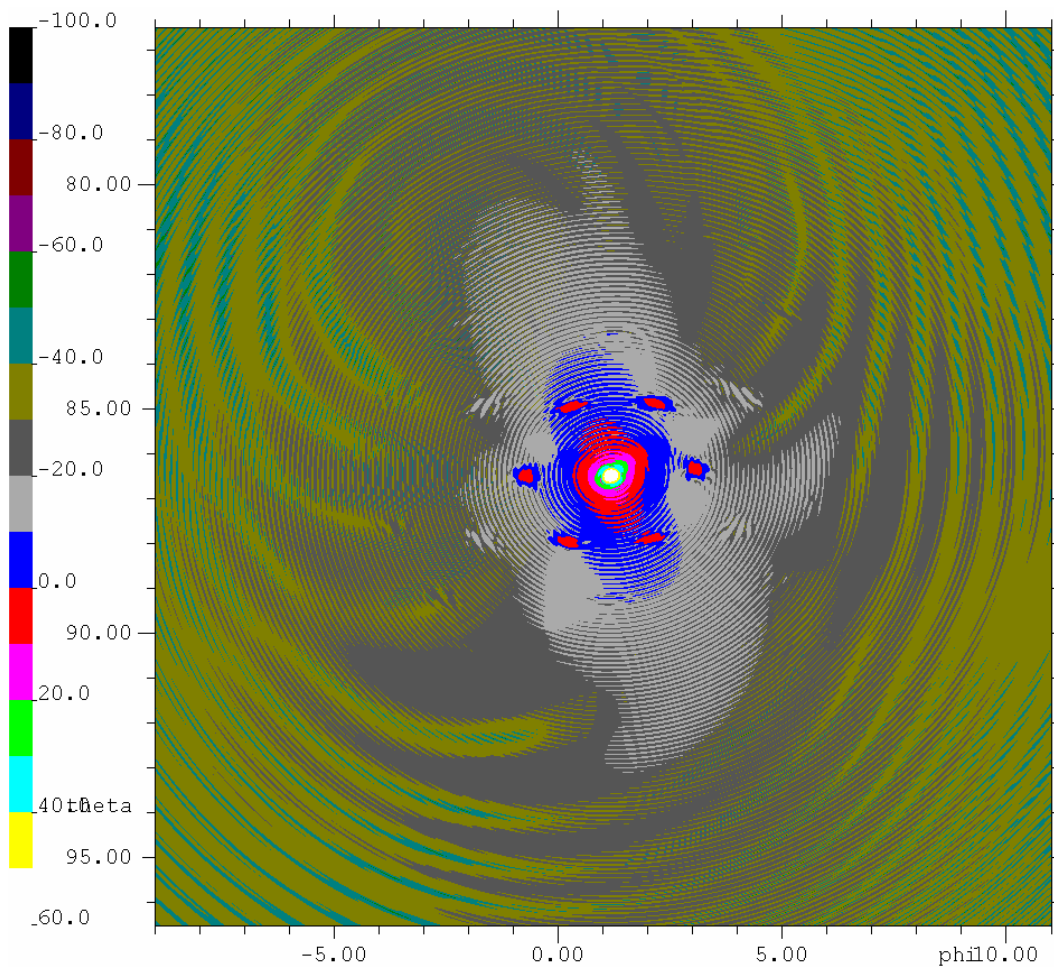


Figure 4-13 Far field from the PLANCK telescope with quilting errors on the secondary mirror surface.

The grating lobes can be clearly identified in the asymmetry plane and in the  $\pm 60^\circ$  direction. The other simulated grating lobes are more evident in the difference pattern shown in Figure 4-14, where the nominal pattern from Figure 2-2 is subtracted. By comparing with the measured difference pattern shown in Figure 4-14 the positions are seen to be the same but the levels are 12 dB larger. Therefore, the measured average quilting peak must be around  $1.5 \mu$ .

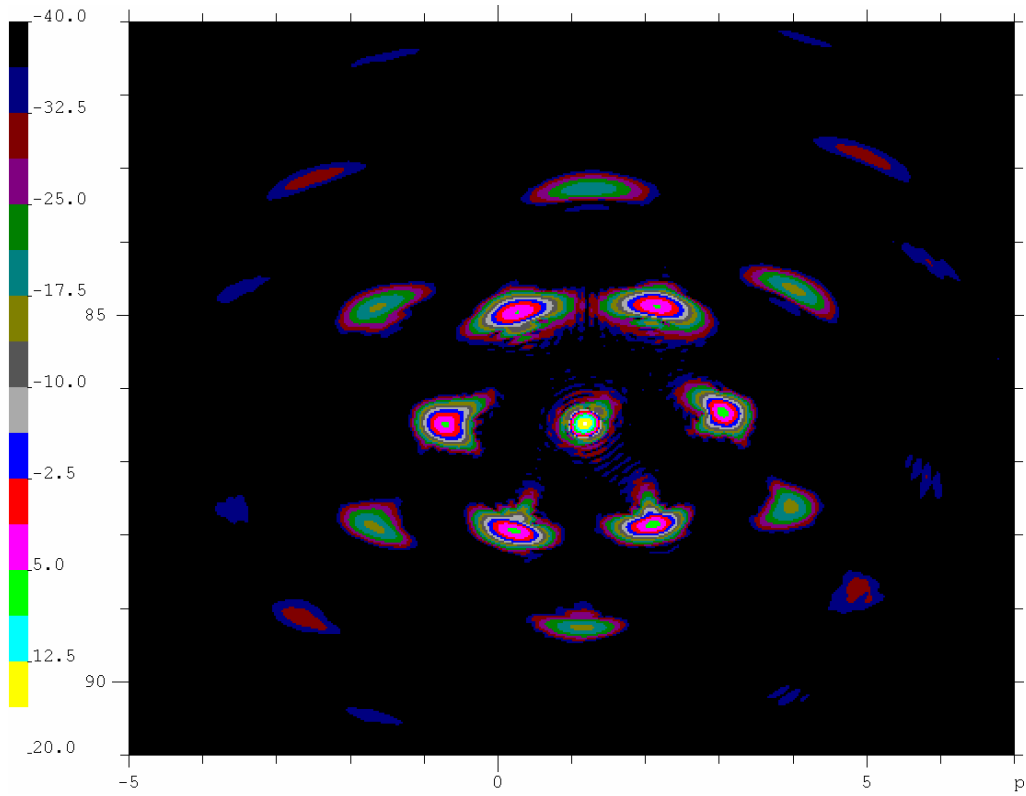


Figure 4-14 Difference field from the PLANCK telescope with quilting errors on the secondary mirror surface.

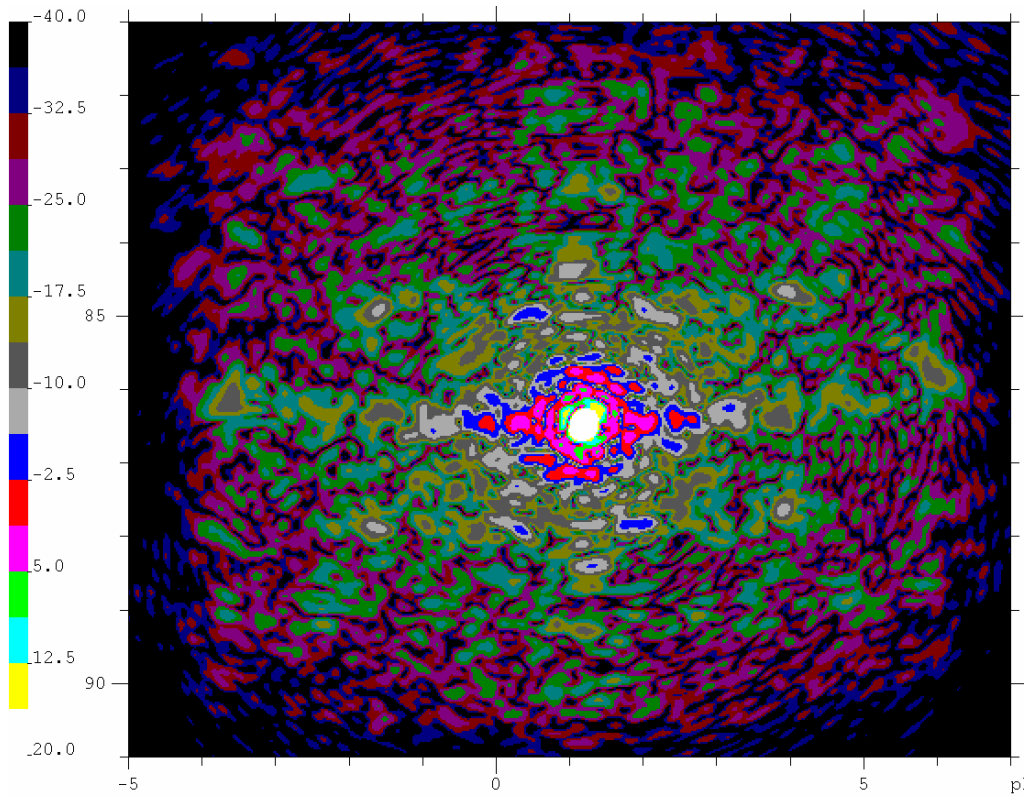


Figure 4-15 Difference field from the PLANCK telescope with measured the secondary mirror surface.

The surface degradation from the handle for the supporting booms is also seen for the secondary mirror in Figure 4-4. The three support points are located in a ring of radius 304 mm in the M2C coordinate system, see TICRA Report S-1247-01, giving the following coordinates of the surface distortion spots:

$X_{M2C}$	$Y_{M2C}$
304.0 mm	0.0 mm
-152.0 mm	263.33 m
-152.0 mm	-263.33 m

The positions recognized in Figure 4-4 are slightly different with centre in y-direction of  $\pm 225$  mm. The size of the spots is approximated to a peak of  $10 \mu$  and a standard deviation of 30 mm. The Gaussian hats are shown in Figure 4-16.

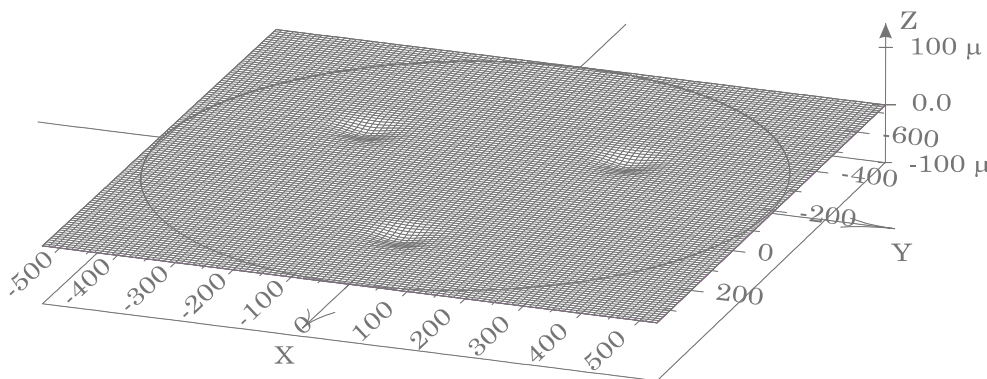


Figure 4-16 Gaussian hats simulating mirror support

These spots will create a broad distortion beam in the peak gain direction with a 3 dB beam width of  $0.8^\circ$  corresponding to a scaled 110 mm spot diameter, see Figure 4-17. The maximum level is 1.7 dBi and the lobes with  $0.2^\circ$  spacing in the  $60^\circ$  planes corresponding to the scaled distances of 456 mm between the spots. The lobes are also shown in Figure 4-18 where the distortion field is plotted together with the nominal pattern.

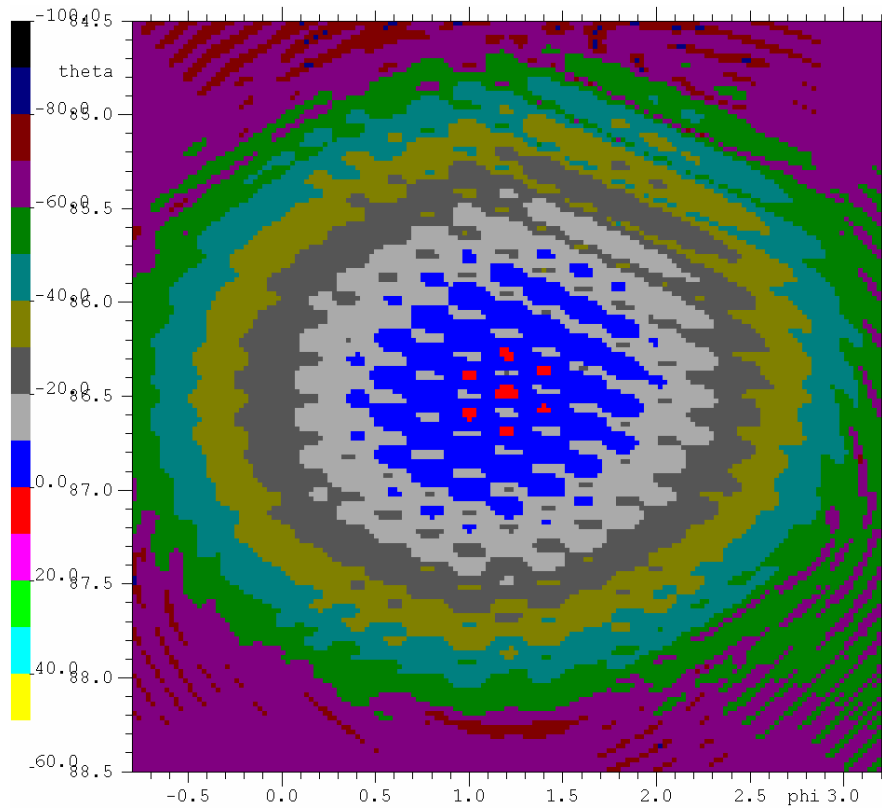


Figure 4-17 Difference field.

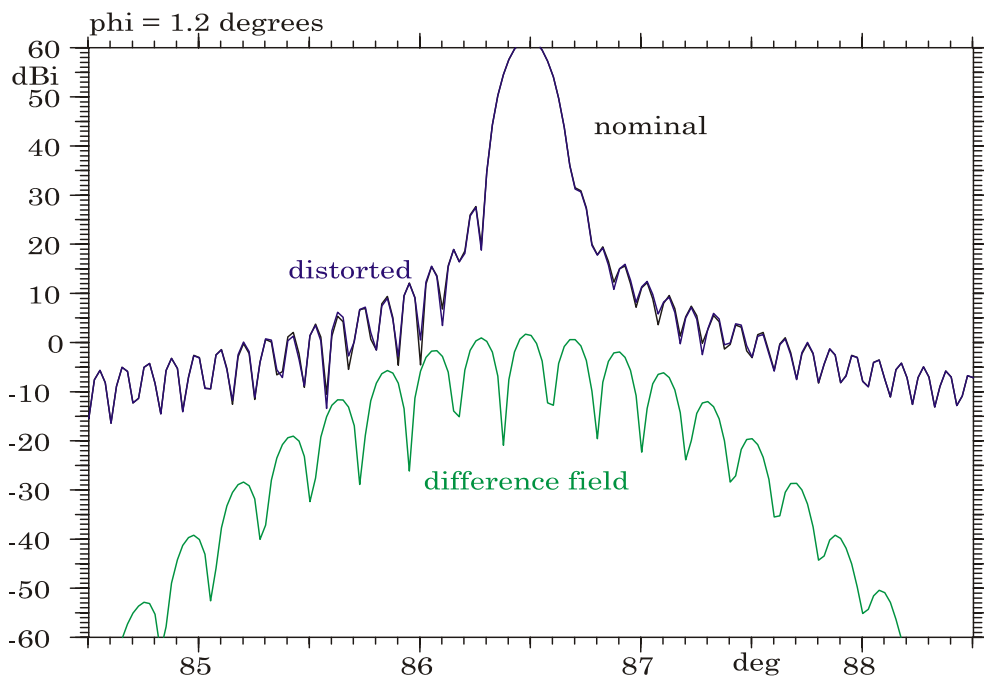


Figure 4-18 Pattern cut for  $\phi = 1,2^\circ$ .

The level of the distortion field is seen to be too small to have any significant influence on the total pattern.

The total distorted and difference pattern in the symmetry plane is shown in Figure 4-19.

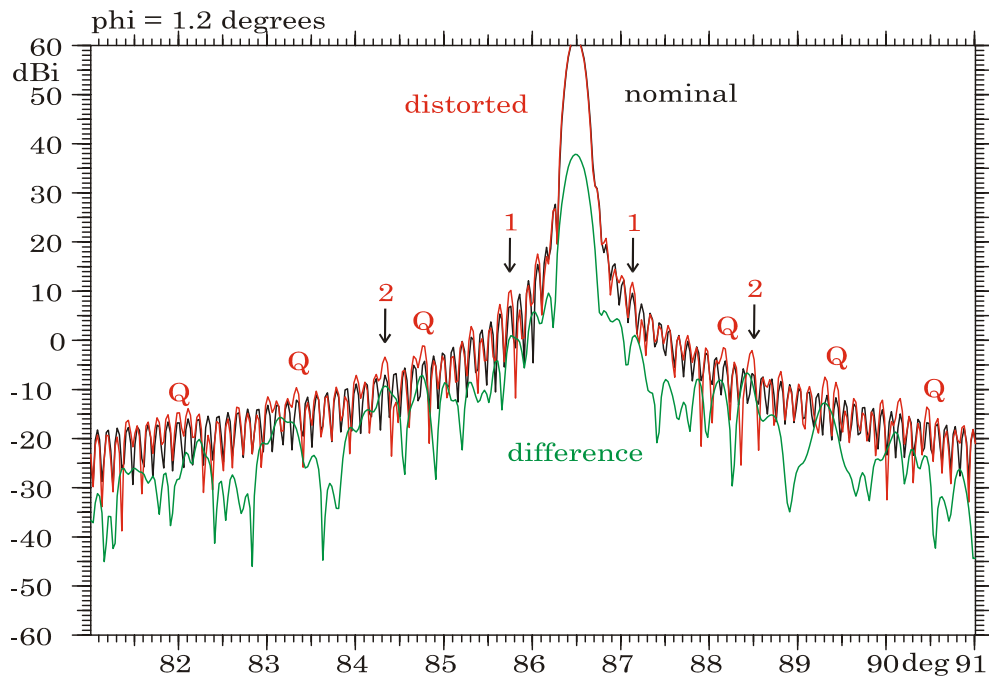


Figure 4-19 Distortion pattern cut for  $\phi = 1,2^\circ$  .

The Quilting sidelobes are marked with an Q. The two sidelobes with index 1 are generated by a surface distortion with a distance of 130 mm. This distortion can be identified in the left side of Figure 4-4 for  $x = 630$  mm and  $x = 500$  mm as a ridge stretching all over the  $y$  range. The distortion may generated sidelobes in a distance of  $n \cdot 0.7^\circ$  and can then also be responsible for the lobes with index 2.

## 5. COMBINED RF PERFORMANCE

The RF performance from both the measured mirrors is presented in the raster plot of Figure 5-1. The main beam is located in the centre of the grid at  $\theta = 86.449^\circ$  and  $\phi = 1.197^\circ$  and shown as a white spot. The colours give the levels of the field with a white maximum of 60 dBi and with colour shifts in 10 dB intervals down to -100 dBi. Everything below -100 dBi is black. Compared to the nominal field in Chapter 2 the aperture degradation gives a beam tilt of  $\Delta\theta = 0.038^\circ$  and  $\Delta\phi = 0.014^\circ$ , and the main beam peak is increased by 0.001 dB to 61.891 dBi. This is possible because the nominal shaped system is not perfect for any of the detectors. The aperture error for one detector beam may then be reduced by the surface degradation.

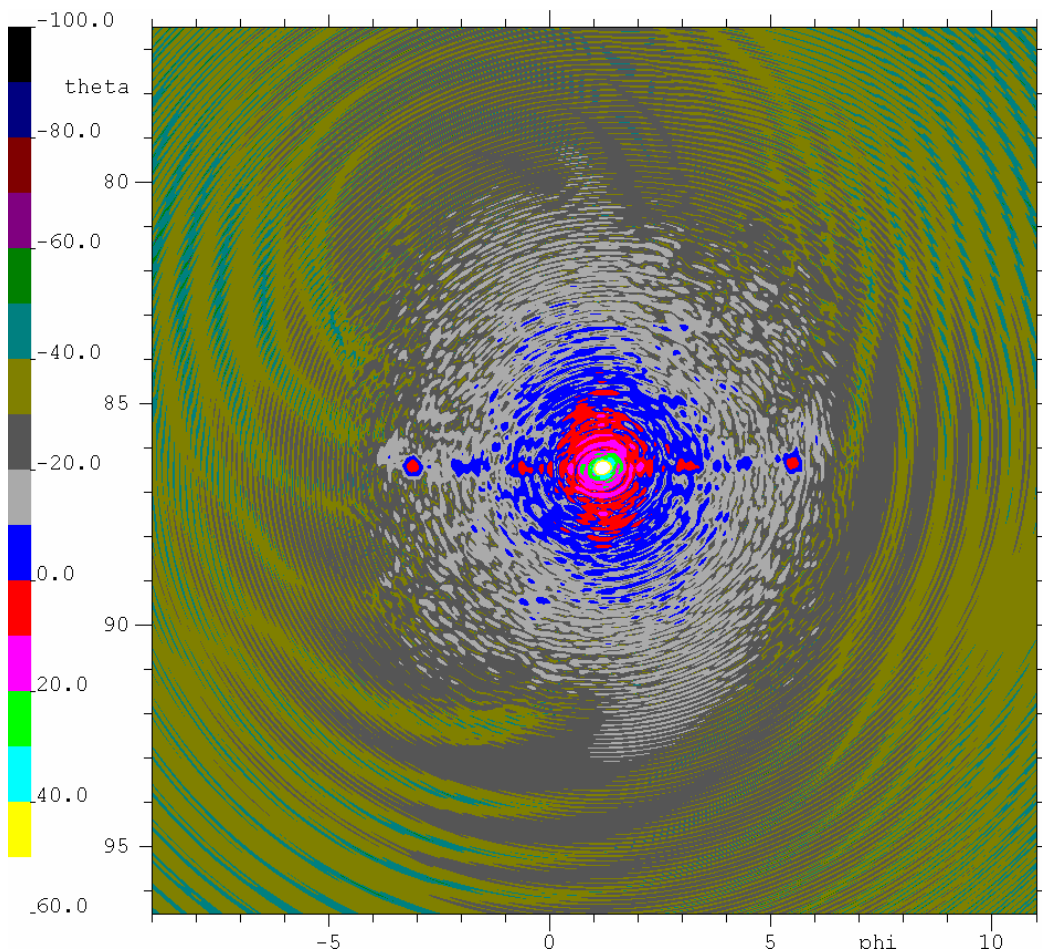


Figure 5-1 Far field from the PLANCK telescope with measured mirrors.

The grating lobes from the primary mirror quilting can be distinguished from the lobes of the secondary mirror quilting on the different angular distance from the main peak. The observed different angles are due to the magnification factor on the distortion periodicity of the secondary mirror, see Figure 4-9. For comparison the RF performance from the quilting distortions on both the secondary and the primary mirror only is calculated in Figure 5-3 with quilting peaks of  $1.5 \mu$  and  $1.6 \mu$ , respectively

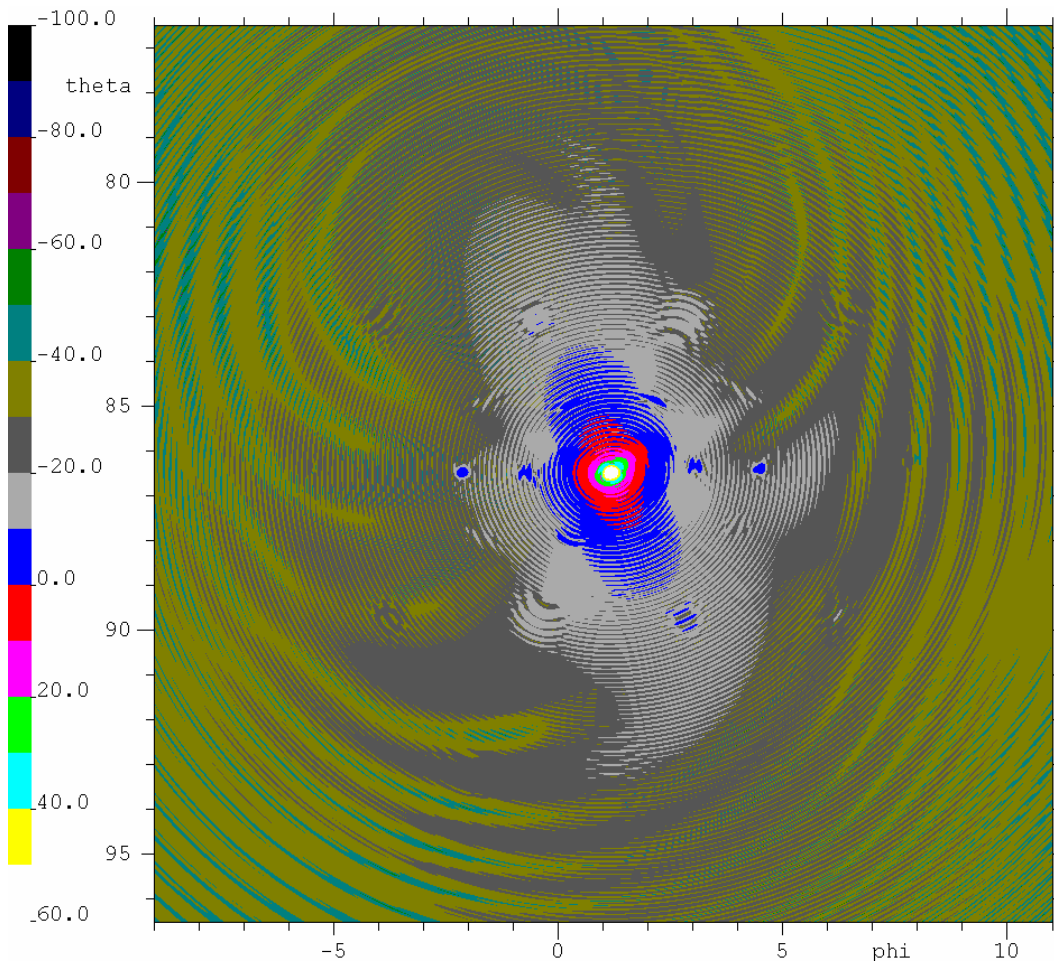


Figure 5-2 Far field from the PLANCK telescope with quilting errors on both mirrors.

A zoomed picture of the degraded far field in the region with the effect from the measured surfaces is shown in Figure 5-4.

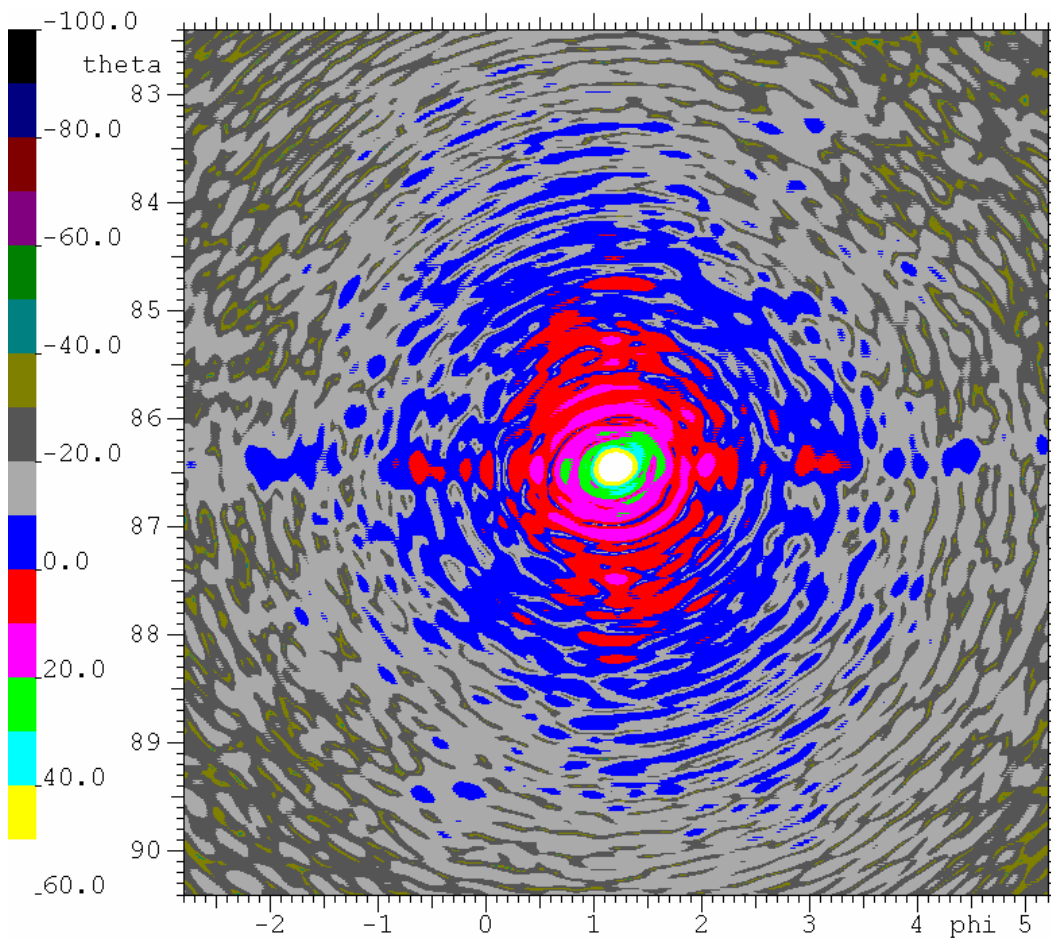


Figure 5-3 Far field from the PLANCK telescope with measured mirrors.

All degradations are mainly in the sidelobe regions whereas the main beam is nearly unchanged. The main beam is compared with the nominal field in Figure 5-4 and Figure 5-5, respectively. The only major change is the beam tilt of  $0.04^\circ$ . Other changes are first remarkable 30 dB below the peak. The Main RF parameters for the two main beams are presented in Table 5.1.

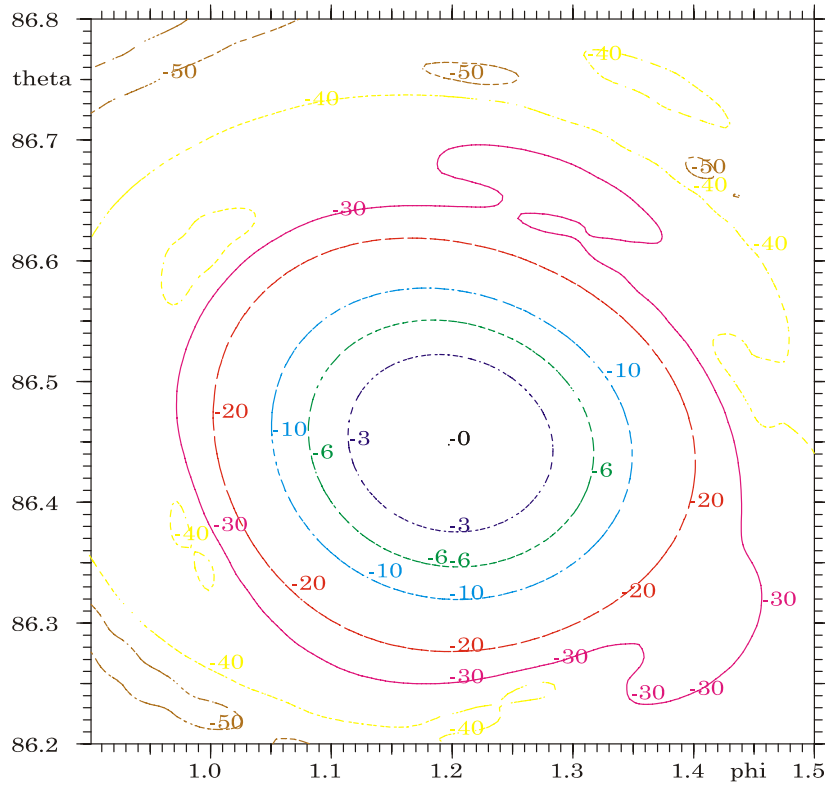


Figure 5-4 Far field from the PLANCK telescope with measured mirrors.

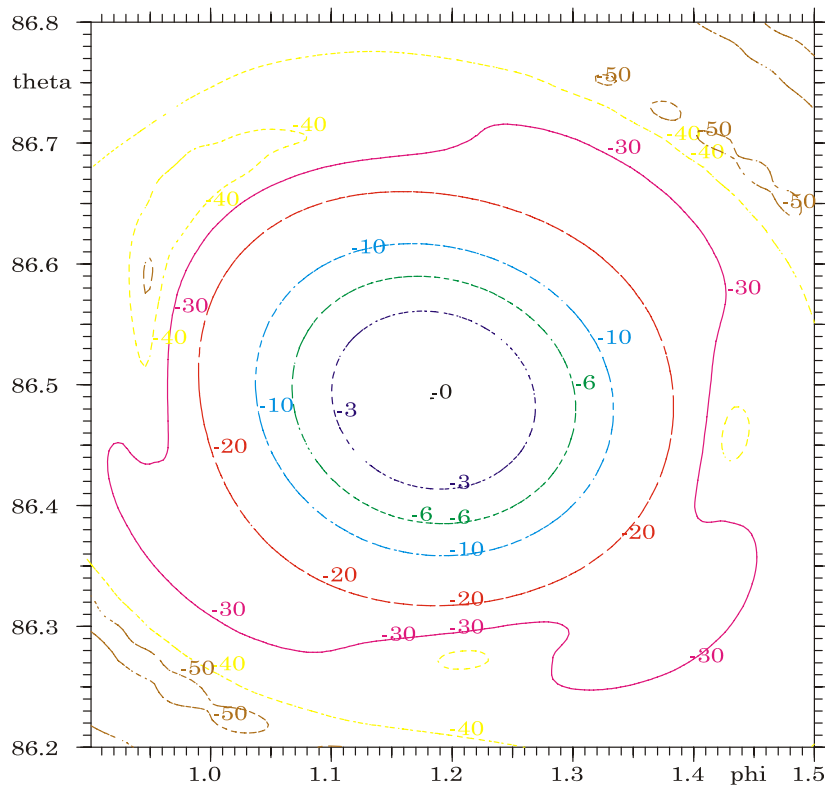


Figure 5-5 Far field from nominal PLANCK telescope with ideal mirrors.

<b>100 GHz horn, HFI100-1</b>	<b>Nominal</b>	<b>Qualifica- tion Model</b>
<b>Peak</b>		
Gain [dBi]	61.890	61.891
Direction in $\theta$	86.487°	86.449°
Direction in $\phi$	1.183°	1.197°
<b>Distance from peak to 3 dB contour</b>		
Min [arcmin]	4.34	4.30
Max [arcmin]	5.11	5.14
<b>Distance from peak to 20 dB contour</b>		
Min [arcmin]	10.19	9.83
Max [arcmin]	12.07	12.27
<b>Power [%]</b>		
inside 3 dB	52.57	52.78
inside 10 dB	91.23	91.45
inside 20 dB	98.48	98.60
<b>Solid angle in steradians*10-6</b>		
Inside 3dB	5.90	5.93
Inside 10 dB	18.28	18.32
Inside 20 dB	32.76	32.50
Angular resolution arcmin	9.42	9.45

Table 5-1 RF characteristics of PLANCK telescope

## REFERENCES

ESA (2000)

“Planck Telescope Design Specification”  
SCI-PT-RS-07024, dated 31/08/00.

ESA (2004)

”Planck Primary & Secondary Reflector Specification”,  
SCI-PT-RS-07422, dated 15-jan-2004.

Per H. Nielsen (2000)

“RF effect of core print-through distortion on the  
PLANCK telescope”, S-801-05, dated Marts, 2000

Per H. Nielsen & Knud Pontoppidan(2003)

“Influence on beam patterns from mirror support distortions”, S-1247-01, dated September 2003.

Per H. Nielsen (2004)

“RF effect of dimpling distortion on the PLANCK telescope”, S-1281-01, dated April 2004.